Gain Form of the Ensemble Transform Kalman Filter and Its Relevance to Satellite Data Assimilation with Model Space Ensemble Covariance Localization

CRAIG H. BISHOP

Marine Meteorology Division, Naval Research Laboratory, Monterey, California

JEFFREY S. WHITAKER

NOAA/Earth System Research Laboratory, Boulder, Colorado

LILI LEI

Nanjing University, Nanjing, China

(Manuscript received 20 April 2017, in final form 7 August 2017)

ABSTRACT

To ameliorate suboptimality in ensemble data assimilation, methods have been introduced that involve expanding the ensemble size. Such expansions can incorporate model space covariance localization and/or estimates of climatological or model error covariances. Model space covariance localization in the vertical overcomes problematic aspects of ensemble-based satellite data assimilation. In the case of the ensemble transform Kalman filter (ETKF), the expanded ensemble size associated with vertical covariance localization would also enable the simultaneous update of entire vertical columns of model variables from hyperspectral and multispectral satellite sounders. However, if the original formulation of the ETKF were applied to an expanded ensemble, it would produce an analysis ensemble that was the same size as the expanded forecast ensemble. This article describes a variation on the ETKF called the gain ETKF (GETKF) that takes advantage of covariances from the expanded ensemble, while producing an analysis ensemble that has the required size of the unexpanded forecast ensemble. The approach also yields an inflation factor that depends on the localization length scale that causes the GETKF to perform differently to an ensemble square root filter (EnSRF) using the same expanded ensemble. Experimentation described herein shows that the GETKF outperforms a range of alternative ETKF-based solutions to the aforementioned problems. In cycling data assimilation experiments with a newly developed *storm-track* version of the Lorenz-96 model, the GETKF analysis root-mean-square error (RMSE) matches the EnSRF RMSE at shorter than optimal localization length scales but is superior in that it yields smaller RMSEs for longer localization length scales.

1. Introduction

Nonvariational ensemble Kalman filters (Houtekamer and Mitchell 1998; Bishop et al. 2001; Anderson 2001; Whitaker and Hamill 2002) are now used across a wide range of fields. Variations on these techniques that involve expanding the ensemble size beyond the K ensemble members propagated by the nonlinear ensemble forecast have been proposed for differing reasons.

Bishop and Hodyss (2009, 2011) introduced ensemble expansion techniques in order to allow flow-dependent time-evolving ensemble covariance localization. These papers used the fact that an ensemble of size K that is expanded to a size of $M = LK$ by taking the element-wise product of each raw-member with each of the L columns of the square root of a localization matrix results in an M-member ensemble whose covariance is inherently localized. We shall hereafter refer to this type of expansion as a modulation product ensemble expansion. Leng et al. (2013) used an equivalent procedure to obtain nonadaptive inherent localization. Whitaker (2016) used a modulation product ensemble expansion to inherently localize ensemble covariances in the vertical and thus avoid the pitfalls outlined in Campbell et al. (2010) of attempting to localize satellite radiance ensemble covariances in radiance space rather than model space.

Corresponding author: Craig H. Bishop, bishop@nrlmry.navy.mil

DOI: 10.1175/MWR-D-17-0102.1

Kretschmer et al.'s (2015) climatologically augmented local ensemble transform Kalman filter (ETKF) expands the ensemble size by introducing M–K climatological forecast error proxies to the raw K forecast error proxies produced by the nonlinear model to create an M-member ensemble. As shown by Bishop and Satterfield (2013), the mean of the distribution of true error variances given an imperfect ensemble variance is a weighted ensemble variance plus a weighted climatological variance. Kretschmer et al.'s innovation allows such hybrid error covariance models to be incorporated directly into the ETKF framework. Sommer and Janjic (2017) tested ensemble expansions similar to Kretschmer et al.'s (2015) but in their case they used them to account for model error.

Regardless of the motivation for using an ensemble of size M to update the ensemble mean while only propagating an ensemble of size K, one is faced with the question of how to create the K analysis perturbations that will be used to initialize the next K-member ensemble forecast. In considering how to do this, one must also account for the fact that when some type of ensemble expansion has been employed, some ensemble perturbations may be considered to be more representative of the true forecast error distribution. For well-tuned ensemble forecasting systems, the most representative ensemble perturbations will be the K ensemble perturbations produced by the nonlinear forecast model. The gain ETKF (GETKF) introduced in this paper, provides a way of producing K analysis ensemble members from an M-member prior ensemble that can account for the fact that the K raw ensemble perturbations are likely better error proxies than arbitrarily selected members of the M-member ensemble. To illustrate the technique, we will focus on the case where the ensemble expansion is used to enable vertical ensemble covariance localization for the assimilation of satellite-like observations that are vertical integrals of the state. Section 2 uses a simple satellite-relevant data assimilation problem to illustrate how (i) the modulation ensemble expansion technique would improve the ability of the ETKF to extract information from satellites but (ii) does *not* provide an obvious solution for the problem of how to create a K-member analysis ensemble from the M-member analysis ensemble produced by the ETKF. Section 3 introduces the GETKF as a solution to this problem. Sections 4 and 5 compare the accuracy of the GETKF method for obtaining K analysis members with various ad hoc methods for obtaining K analysis members from the ETKF's M analysis members. Section 4 makes the comparison using statistical models and theoretically derived *true* analysis error covariance matrices while section 5 makes the comparison within the context of a newly developed *storm-track* version of the Lorenz-96 model and a cycling data assimilation scheme. Concluding remarks follow in section 6.

2. ETKF satellite data assimilation and modulated ensembles

a. Modulated ensembles

Consider the problem of estimating a $n = 100$ gridpoint vertical profile of temperature from $p = 100$ satellite radiances whose vertical weighting functions are depicted in Fig. 1. Methods of localizing ensemble covariances in the vertical based on the distances between observations and model variables (Hamill et al. 2001) are inappropriate for such observations because the variable that is observed does not exist at a single height: each observation is an integral of variables at many different heights. Campbell et al. (2010) compared the performance of EnKFs that used model space vertical covariance localization, in which the localization is prescribed purely in terms of the distance between model variables, and EnKFs that used observation space localization, in which the localization is based on "estimated" distances between satellite observations and other variables. They found that the model space localization was superior to the observation space localization. In particular, the observation space localization approach was unable to recover the true state in the special case where there are as many perfect satellite observations as there are model variables. In contrast, with model space localization, EnKFs were readily able to recover the true model state in this case.

Bishop and Hodyss (2009) showed that an easy way of incorporating model space localization within an ETKF-type data assimilation scheme is to recognize that if the $n \times L$ matrix $\mathbf{W} = [\mathbf{w}_1, \mathbf{w}_2, \ldots, \mathbf{w}_L]$ is a square root of a model space localization matrix $\mathbf{F} = \mathbf{W}\mathbf{W}^{\mathrm{T}} = \sum_{i=1}^{L} \mathbf{w}_i \mathbf{w}_i^{\mathrm{T}}$ and the $n \times K$ matrix $\mathbf{U} = [\mathbf{u}_1, \mathbf{u}_2, \ldots, \mathbf{u}_K] = 1/\sqrt{K-1}[\mathbf{x}'^f_1, \mathbf{x}'^f_2, \ldots, \mathbf{x}'^f_K] = \mathbf{X}'^f/\sqrt{K-1}$ is a square root of the unlocalized ensemble covariance matrix $\mathbf{P}^f_{\mathrm{ens}} = \mathbf{U}\mathbf{U}^{\mathrm{T}} = \sum_{j=1}^{K} \mathbf{u}_j \mathbf{u}_j^{\mathrm{T}} = 1/(K-1)\sum_{j=1}^{K} \mathbf{x}'^f_j (\mathbf{x}'^f_j)^{\mathrm{T}}$, where $\mathbf{x}'^f_j = \mathbf{x}^f_j - (1/K)\sum_{j=1}^{K} \mathbf{x}^f_j$ is the jth raw ensemble perturbation corresponding to the jth ensemble forecast member $\mathbf{x}^f_j$, then the localized ensemble covariance matrix is given by

$$\mathbf{P}^f_{\mathrm{loc}} = \mathbf{P}^f_{\mathrm{ens}} \odot \mathbf{F} = \mathbf{Z}\mathbf{Z}^{\mathrm{T}}, \tag{1}$$

where the symbol $\odot$ defines the Schur elementwise matrix/vector product and where the square root $\mathbf{Z}$ of $\mathbf{P}^f_{\mathrm{loc}}$ is a $n \times (KL)$ matrix given by the modulation product ($\triangle$) of $\mathbf{U}$ by $\mathbf{W}$ defined by

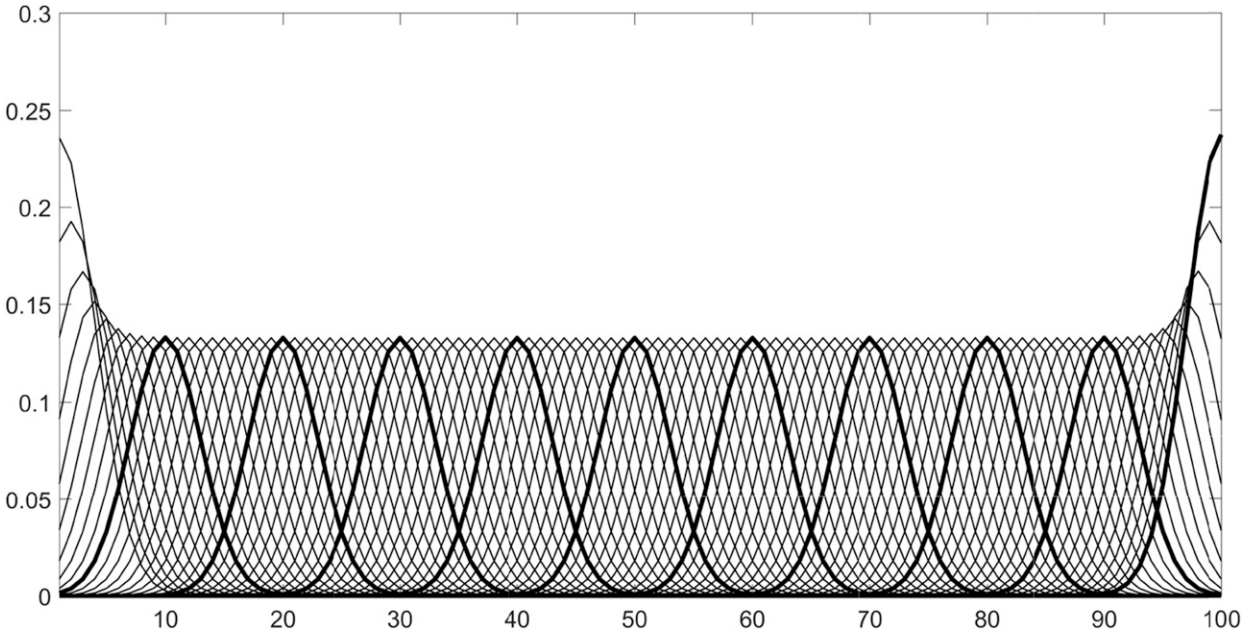

FIG. 1. Many satellites observe weighted vertical integrals of the atmospheric state. Here, we consider satellite-like observations that are weighted vertical integrals of the state of an idealized data assimilation model. The abscissa axis gives this model's vertical level while the ordinate axis gives the weights used in the vertical integral. Each distinct line in the above diagram depicts the set of weights used to vertically integrate the state to create a satellite-like observation. The sum of the weights associated with each observation is equal to unity. The weighting functions associated with every 10th observation have been plotted with a thick line in order to make it easier to distinguish the shape of individual weighting functions (each weighting function has a single peak). There are 100 distinct observations: one for each model level.

$$\mathbf{Z} = \mathbf{W} \triangle \mathbf{U} = [(\mathbf{w}_1 \odot \mathbf{u}_1, \mathbf{w}_1 \odot \mathbf{u}_2, \ldots, \mathbf{w}_1 \odot \mathbf{u}_K), \ldots, (\mathbf{w}_L \odot \mathbf{u}_1, \mathbf{w}_L \odot \mathbf{u}_2, \ldots, \mathbf{w}_L \odot \mathbf{u}_K)]. \quad (2)$$

The expansion of the ensemble size is evident from (2): $\mathbf{Z}$ has $M = KL$ ensemble members whereas $\mathbf{U}$ only has K ensemble members. In the case examined by Whitaker (2016), the modulation product pertained strictly to a vertical localization covariance matrix and $L \sim O(10)$ and hence the modulation product ensemble was an order of magnitude larger than the raw ensemble. The proof that the expanded ensemble given by (2) satisfies (1) is given in Eqs. (1) and (2) of Bishop and Hodyss (2009).

As an illustration of this modulation product ensemble expansion procedure, suppose that the element in the ith row and jth column of the true $n \times n$ forecast error covariance matrix $\mathbf{P}$ is given by

$$\{\mathbf{P}\}_{ij} = \sqrt{\frac{ij}{n^2}} \exp\left[-\frac{1}{2}\left(\frac{i-j}{d_1}\right)^2\right] + \sqrt{\left(1-\frac{i}{n}\right)\left(1-\frac{j}{n}\right)} \exp\left[-\frac{1}{2}\left(\frac{i-j}{d_2}\right)^2\right], \quad (3)$$

with $n = 100, d_1 = 1,$ and $d_2 = 8$. With this setup, as can be seen from Fig. 2a, the error correlation length scale is larger between variables situated in the lower atmosphere (small values of i and j) than the upper atmosphere. With (3) as the true forecast error covariance matrix, we can obtain a reasonable counterpart for the $n \times K$ matrix $\mathbf{X}^f$ of K raw forecast ensemble perturbations using

$$\mathbf{X}^f = \mathbf{P}^{1/2}[\text{randn}(n, K)], \quad (4)$$

where $[\text{randn}(n, K)]$ is an $n \times K$ matrix whose elements are random independent draws from a normal distribution with mean zero and variance 1. Using (4), a $K = 50$ member ensemble was generated and then its (unlocalized) covariance matrix $\mathbf{P}^f_{\text{ens}}$ was plotted in Fig. 2b. Comparing Figs. 2b and 2a, it is easy to see that the ensemble covariance elements far from the diagonal differ markedly from the true forecast error covariance matrix. An effective way of suppressing these spurious correlations is to take the elementwise (Schur) product of $\mathbf{P}^f_{\text{ens}}$ with the localization matrix $\mathbf{F}$ depicted in Fig. 2c to obtain the localized ensemble covariance $\mathbf{P}^f_{\text{loc}}$ shown in Fig. 2d. Comparison of Figs. 2d, 2a, and 2b shows that

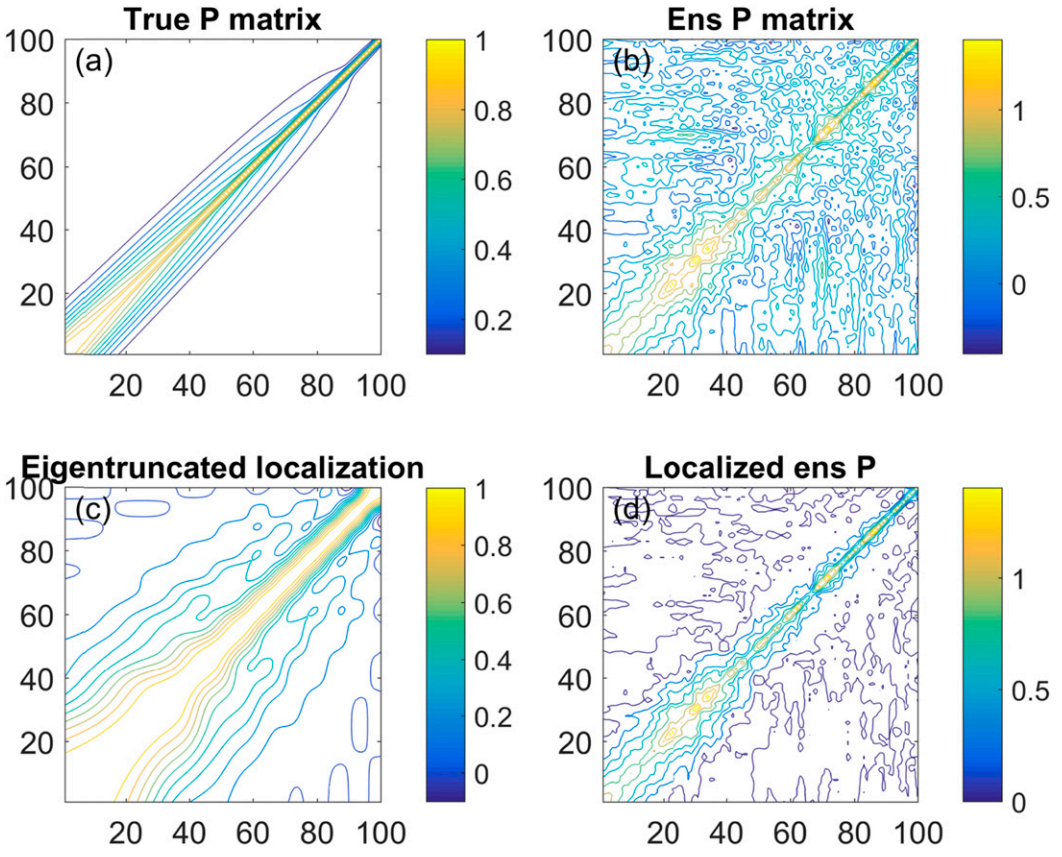

FIG. 2. (a) The true forecast error covariance matrix $\mathbf{P}$. (b) The sample covariance matrix from a 50-member ensemble $\mathbf{P}^f_{\text{ens}}$. (c) The low-rank localization matrix $\mathbf{F}$ obtained from a high-rank localization matrix by only using the top 10 eigenvectors and eigenvalues of the high-rank localization matrix and then renormalizing those eigenvectors to ensure that each diagonal element of the low-rank localization matrix $\mathbf{F}$ is equal to 1. (d) The localized ensemble covariance matrix $\mathbf{P}^f_{\text{loc}} = \mathbf{P}^f_{\text{ens}} \odot \mathbf{F}$. The ranges of the color scales indicate the range of the displayed field.

the elements of $\mathbf{P}^f_{\text{loc}}$ far from the diagonal are much more similar to those of the true $\mathbf{P}$ than those of the unlocalized $\mathbf{P}^f_{\text{ens}}$. Note that the localization matrix $\mathbf{F}$ has similar overall characteristics to $\mathbf{P}$ but broader length scales. It was created by the following three steps:

(i) Broader length scales defined by $\tilde{d}_1 = 3d_1$ and $\tilde{d}_2 = 3d_2$ were used in (3) to create a correlation matrix $\tilde{\mathbf{F}}$ that was similar to $\mathbf{P}$ but with broader length scales.

(ii) The eigenvectors and eigenvalue pairs of $\tilde{\mathbf{F}}$ were computed and ordered from largest eigenvalue to smallest eigenvalue. Having determined that only 10 eigenvalues were sufficient to account for 85% of the sum of all the eigenvalues, the 10 leading (eigenvector, eigenvalue) pairs were used to create a low-rank approximation $\tilde{\mathbf{F}}_{\text{low rank}} = \tilde{\mathbf{W}}\tilde{\mathbf{W}}^{\text{T}}$ to $\tilde{\mathbf{F}}$. Note that each column of $\tilde{\mathbf{W}}$ is an eigenvector of $\tilde{\mathbf{F}}$ multiplied by the square root of its corresponding eigenvalue.

(iii) The final low-rank localization matrix $\mathbf{F}$ was created by removing the deviation of the diagonal of $\tilde{\mathbf{F}}_{\text{low rank}}$ from unity using $\mathbf{F} = [\text{diag}(\tilde{\mathbf{F}}_{\text{low rank}})]^{-1/2}\tilde{\mathbf{F}}_{\text{low rank}}[\text{diag}(\tilde{\mathbf{F}}_{\text{low rank}})]^{-1/2} = \mathbf{W}\mathbf{W}^{\text{T}}$, where $\mathbf{W} = \{[\text{diag}(\tilde{\mathbf{F}}_{\text{low rank}})]^{-1/2}\tilde{\mathbf{W}}\}$.

The first three columns $[\mathbf{w}_1, \mathbf{w}_2, \mathbf{w}_2]$ of $\mathbf{W}$ corresponding to the three largest eigenvalues are plotted in Fig. 3.

Figure 3 allows us to visualize the relationship between the raw ensemble members and the modulated ensemble members. Referring to (2), the first K members of the modulated ensemble are $(\mathbf{w}_1 \odot \mathbf{u}_1, \mathbf{w}_1 \odot \mathbf{u}_2, \ldots, \mathbf{w}_1 \odot \mathbf{u}_K)$; hence, they are simply the raw perturbations modulated by an elementwise product with $\mathbf{w}_1$. Figure 3a shows that the main effect of this modulation would be to attenuate the amplitude of the raw perturbations in the upper atmosphere. The second set of K members in the modulated ensemble are given by $(\mathbf{w}_2 \odot \mathbf{u}_1, \mathbf{w}_2 \odot \mathbf{u}_2, \ldots, \mathbf{w}_2 \odot \mathbf{u}_K)$. Figure 3b shows that these perturbations have the opposite sign of the original perturbations in the lower atmosphere and the same sign as the original perturbations in the upper

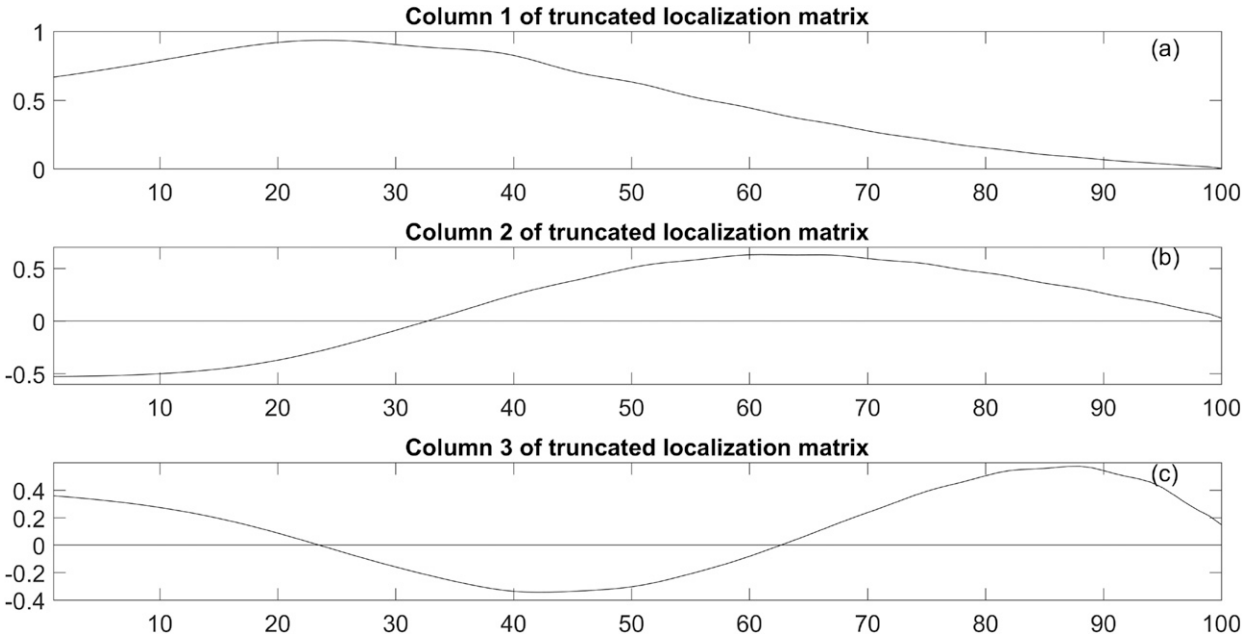

FIG. 3. The first three columns of the square root **W** of the low-rank localization matrix **F**.

atmosphere. Figure 3c shows that unlike the first and second sets, which have zero amplitude at the top of the atmosphere, this third set retains some of the amplitude of the original perturbations at the top of the atmosphere. In addition, Fig. 3c shows that this third set of perturbations will have zero amplitude at two intermediate locations in the vertical. Comparison of all the panels in Fig. 3 shows that columns of **W** have a sinusoidal nature with the associated wavenumber (wavelength) becoming larger (smaller) as the index of the column is increased. With this in mind, a qualitative picture of how the modulated ensemble members differ from the original ensemble members is realized.

Note that a sufficient condition for the mean of the modulated ensemble perturbations to be equal to zero is that the mean of the raw ensemble perturbations be zero. To see this, note that

$$\sum_{k=1}^{M}\mathbf{z}_k = \sum_{i=1}^{L}\sum_{j=1}^{K}\mathbf{u}_j\odot\mathbf{w}_i = \sum_{i=1}^{L}\left(\sum_{j=1}^{K}\mathbf{u}_j\right)\odot\mathbf{w}_i = \mathbf{0}, \text{ provided } \sum_{j=1}^{K}\mathbf{u}_j = \sum_{j=1}^{K}\frac{\mathbf{x}'^{f}_j}{\sqrt{K-1}} = \mathbf{0}. \tag{5}$$

Hence, one can use the M modulated ensemble perturbations to create an M-member ensemble $\mathbf{V}^f = [\mathbf{v}_1^f, \mathbf{v}_2^f, \ldots, \mathbf{v}_M^f]$ that has the same mean as the original ensemble using

$$\mathbf{v}_k^f = \left(\frac{1}{K}\sum_{j=1}^{K}\mathbf{x}_j^f\right) + (\sqrt{M})\mathbf{z}_k. \tag{6}$$

The ensemble given by (6) then has a mean and covariance that satisfy

$$\overline{\mathbf{v}}^f = \frac{1}{M}\sum_{i=1}^{M}\mathbf{v}_i^f = \frac{1}{K}\sum_{j=1}^{K}\mathbf{x}_j^f = \overline{\mathbf{x}}^f \quad \text{and} \quad \frac{\sum_{i=1}^{M}(\mathbf{v}_i^f-\overline{\mathbf{v}}^f)(\mathbf{v}_i^f-\overline{\mathbf{v}}^f)^{\mathrm{T}}}{M} = \mathbf{P}^f_{\mathrm{loc}}, \tag{7}$$

respectively. In other words, while the $M = KL$ members of the modulated ensemble have the same mean as the original ensemble, they have a covariance equal to that of the localized ensemble covariance. This has been confirmed to machine precision for the localized ensemble covariance depicted in Fig. 2d.

b. *The modulated ETKF (METKF) and the analysis ensemble reduction problem*

A key computational step in using the ETKF (Bishop et al. 2001) and its local variation (LETKF; Hunt et al. 2007) to assimilate p observations with an M member ensemble is to compute the matrix

$$\mathbf{A} = (\tilde{H}\mathbf{Z})^{\mathrm{T}}(\tilde{H}\mathbf{Z}), \quad \text{where}$$
$$\tilde{H}\mathbf{Z} = \frac{\mathbf{R}^{-1/2}\{[H(\mathbf{v}_1^f) - \overline{H(\mathbf{v}^f)}], [H(\mathbf{v}_2^f) - \overline{H(\mathbf{v}^f)}], \ldots, [H(\mathbf{v}_M^f) - \overline{H(\mathbf{v}^f)}]\}}{\sqrt{M}}, \quad \text{and}$$
$$\overline{H(\mathbf{v}^f)} = \frac{1}{M}\sum_{i=1}^{M} H(\mathbf{v}_i^f), \tag{8}$$

where H is the (nonlinear) observation operator, $\mathbf{R}$ is the $p \times p$ observation error covariance matrix, and $\tilde{H} = \mathbf{R}^{-1/2}H$ is a normalized nonlinear observation operator. Ignoring the relatively small cost ($\sim Mp$ operations) of computing the normalized observation space ensemble perturbations $\tilde{H}\mathbf{Z}$, the number of operations required to compute the matrix $\mathbf{A}$ is proportional to M^2p. The ETKF uses the eigenvector decomposition:

$$\mathbf{A} = \mathbf{C}\boldsymbol{\Gamma}\mathbf{C}^{\mathrm{T}}, \tag{9}$$

where $\mathbf{C}$ is the orthonormal eigenvector matrix and $\boldsymbol{\Gamma}$ is a diagonal matrix of corresponding eigenvalues. The cost of computing (9) is proportional to M^3. The ETKF estimate of the covariance of the distribution of truth after the assimilation of observations [Eq. (18a) in Bishop et al. (2001)] follows from the singular value decomposition, $\tilde{H}\mathbf{Z} = \mathbf{E}\boldsymbol{\Gamma}^{1/2}\mathbf{C}$, and a careful handling of the vectors associated with zero singular values; it is given by

$$\begin{aligned}\mathbf{P}^a_{\mathrm{METKF}} &= \mathbf{Z}\mathbf{Z}^{\mathrm{T}} - \mathbf{Z}(\tilde{H}\mathbf{Z})^{\mathrm{T}}[(\tilde{H}\mathbf{Z})(\tilde{H}\mathbf{Z})^{\mathrm{T}} + \mathbf{I}]^{-1}(\tilde{H}\mathbf{Z})\mathbf{Z}^{\mathrm{T}} \\ &= \mathbf{Z}\mathbf{C}(\boldsymbol{\Gamma} + \mathbf{I})^{-1}\mathbf{C}^{\mathrm{T}}\mathbf{Z}^{\mathrm{T}} = \mathbf{Z}^a\mathbf{Z}^{a\mathrm{T}},\end{aligned} \tag{10}$$

where the subscript METKF stands for modulated ETKF and where

$$\mathbf{Z}^a = \mathbf{Z}[\mathbf{C}(\boldsymbol{\Gamma} + \mathbf{I})^{-1/2}\mathbf{C}^{\mathrm{T}}] \quad \text{and}$$
$$\tilde{H}\mathbf{Z}^a = (\tilde{H}\mathbf{Z})[\mathbf{C}(\boldsymbol{\Gamma} + \mathbf{I})^{-1/2}\mathbf{C}^{\mathrm{T}}] \tag{11}$$

give the METKF analysis perturbations in model and observation space, respectively; in addition, the posterior mean of the distribution of truth is given by

$$\overline{\mathbf{v}}^a = \overline{\mathbf{v}}^f + \mathbf{Z}^a(\tilde{H}\mathbf{Z}^a)^{\mathrm{T}}[\mathbf{R}^{-1/2}\mathbf{y} - \overline{\tilde{H}\mathbf{v}^f}]. \tag{12}$$

Note that (12) implicitly incorporates the localization matrix $\mathbf{F}$. Furthermore, note that if $\mathbf{F}$ was the rank one matrix in which all elements are equal to 1 then (12) would give a posterior mean identical to that which would be obtained from an ETKF with no localization and no modulated ensemble.

The performance advantages of such implicit vertical localization over no localization can be illustrated using our idealized error model. We first generate a true state $\mathbf{x}^t$ using

$$\mathbf{x}^t = \mathbf{P}^{1/2}[\mathrm{randn}(n, 1)]. \tag{13}$$

Comparison of (13) with (4) makes it clear that (13) ensures that our raw ensemble members are drawn from the same distribution as the truth. We then generate $p = 100$ true observations using $\mathbf{y}^t = \mathbf{H}\mathbf{x}^t$, where each row of $\mathbf{H}$ is one of the weighting functions shown in Fig. 1. To create relatively accurate but error-prone observations $\mathbf{y}$ of known observation error covariance $\mathbf{R}$ from these true observations, we let

$$\mathbf{R} = \frac{1}{64}[\mathrm{diag}(\mathbf{H}\mathbf{P}\mathbf{H}^{\mathrm{T}})], \tag{14}$$

where $[\mathrm{diag}(\mathbf{H}\mathbf{P}\mathbf{H}^{\mathrm{T}})]$ is the diagonal matrix formed from the diagonal elements of the matrix $\mathbf{H}\mathbf{P}\mathbf{H}^{\mathrm{T}}$, and then we let

$$\mathbf{y} = \mathbf{y}^t + \mathbf{R}^{1/2}[\mathrm{randn}(p, 1)]. \tag{15}$$

Employing a raw ensemble generated using (4), (12) was used to estimate the true posterior mean with and without the use of a modulated ensemble. The unmodulated or raw ensemble case was simply achieved by replacing the $\mathbf{F}$ localization matrix depicted in Fig. 2c by the rank one matrix whose elements are all equal to unity.

The blue line in Fig. 4a depicts an example of a true model state generated using (13). In Fig. 4b, the blue line depicts the corresponding true state in observation space while the red line depicts the corresponding error-prone observations and the cyan line depicts the mean of the forecast ensemble in observation space. The difference between the observations (Fig. 4b, red line) and the prior mean in observation space (Fig. 4b, cyan line) is then used in (12) to correct the model space prior ensemble mean (Fig. 4a, cyan line). The resulting analyses obtained with and without a modulated ensemble are depicted in Fig. 4a by the mauve and black lines, respectively. Inspection of Fig. 4a shows that the

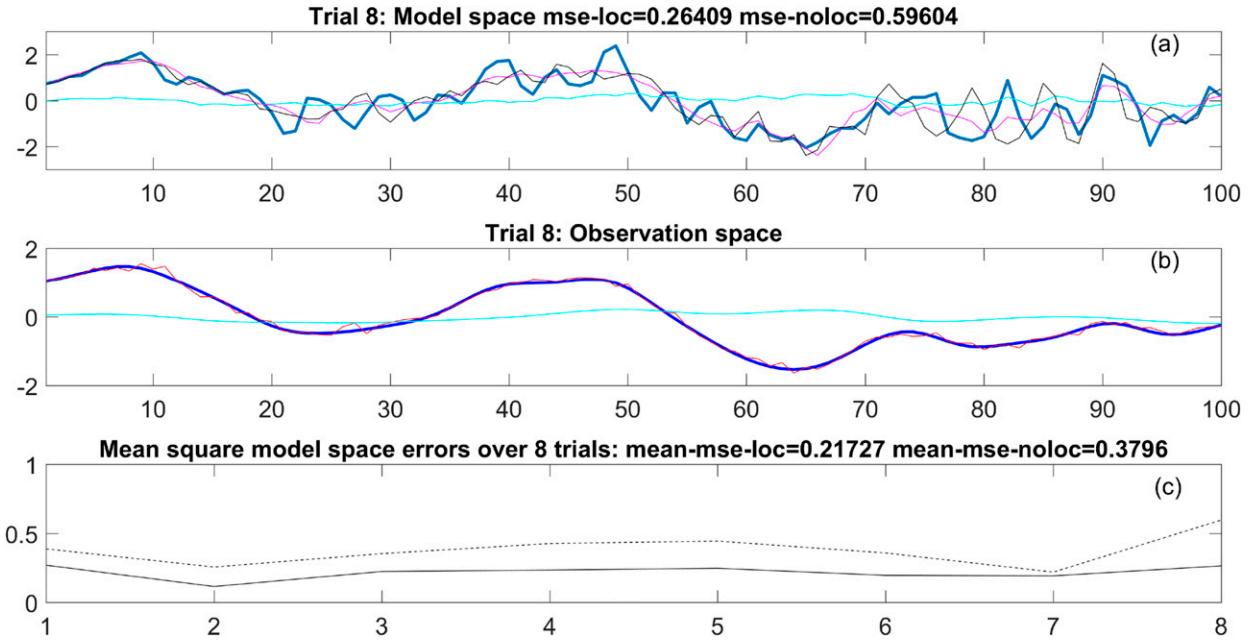

FIG. 4. Data assimilation setup and performance. (a) The blue and cyan lines, respectively, give the model space truth and prior mean, while the mauve and black lines give the ETKF analysis mean with and without modulated ensembles, respectively. (b) The blue and red lines give the observation space truth and error-prone observations, respectively, while the cyan line gives the observation space prior mean. (c) The solid and dashed lines, respectively, give the MSE of the ETKF with and without localization during eight independent trials. Note that the abscissa in (a) refers to the model index, in (b) it refers to the observation index, and in (c) it refers to the index of an independent trial.

$M = KL = 500$ member modulated ensemble allows the analysis (mauve line) to track the true state (blue line) more closely than the analysis (black line) from the unmodulated $K = 50$ member ensemble. Direct computation shows that, in this case, the mean square errors (MSEs) of the analyses with and without the modulated ensembles are 0.26 and 0.6, respectively. To check whether this difference was statistically significant, the aforementioned data assimilation experiment was repeated eight times using entirely independent random numbers to create the truth, the observations, and the ensemble. The dashed and solid lines give the MSEs for the unmodulated and modulated ensemble cases, respectively, in each of these eight experiments. In all eight cases, the MSE obtained using the modulated ensemble was lower than that obtained using the unmodulated ensemble. If there were no statistical difference in ETKF performance with and without modulated ensembles, then the probability of finding superior performance in eight out of eight cases would be $2^{-8} \approx 0.004$ and hence this null hypothesis can be rejected with more than 99% confidence. Considering all eight of the cases, the mean MSEs with and without the modulated ensemble were 0.22 and 0.38, respectively. Thus, this idealized example provides a simple illustration of how the implicit model space localization imparted by the modulated ensembles fundamentally improves the ability of the ETKF to extract information from accurate satellite-like observations.

An unrealistic aspect of our simple model is the fact that it only represents a single-model vertical column. In practical applications of the ETKF, one uses the local form (Hunt et al. 2007) to allow all observations from a neighboring observation volume to update some variables at the center of the observation volume. Localization is typically achieved by computing the separation distances between observations and the model variables being updated, and then, either artificially increasing observation error variance with increasing separation distance and/or by excluding observations whose separation distance exceeds a critical value. Without the implicit vertical localization imparted via modulation product ensemble expansion, one would typically only update the variables at a single grid point with each application of the ETKF. When there are many observations distributed in the vertical, this approach makes for redundant calculations, as there are a large number of observations that are common to each observation volume. The vertical covariance localization via modulation product ensemble expansion approach described here opens up the possibility of using LETKF observation volumes to simultaneously update entire vertical columns of variables while still applying localization at

each level. Within this framework, model space vertical ensemble covariance localization is obtained through the use of a modulation product while horizontal localization would be obtained using standard LETKF localization techniques such as distance-dependent observation error variance inflation and/or some sort of distance-dependent observation exclusion procedure (Hunt et al. 2007). For this case, the METKF update can be written in the form

$$\mathbf{S}_j\overline{\mathbf{v}}^a = \mathbf{S}_j\overline{\mathbf{v}}^f + (\mathbf{S}_j\mathbf{Z})[\mathbf{C}(\mathbf{\Gamma}+\mathbf{I})^{-1}\mathbf{C}^{\mathrm{T}}](\tilde{H}_j\mathbf{Z})^{\mathrm{T}}[\mathbf{R}_j^{-1/2}\mathbf{y} - \overline{\tilde{H}_j\mathbf{v}^f}] \tag{16}$$

for the ensemble mean, where $\mathbf{S}_j$ selects the n model variables associated with the jth vertical column of the model, $\tilde{H}_j$ is the observation operator associated with the corresponding jth observation volume, and $\mathbf{R}_j$ is the observation error covariance matrix for these observations. (Recall that the observation error variances in $\mathbf{R}_j$ may be artificially inflated with distance from the central column being updated.) For the individual ensemble members,

$$\mathbf{S}_j\mathbf{V}^a_{\mathrm{loc}} = (\mathbf{S}_j\overline{\mathbf{v}}^a)\mathbf{1}_M^{\mathrm{T}} + (\sqrt{M})(\mathbf{S}_j\mathbf{Z})[\mathbf{C}(\mathbf{\Gamma}+\mathbf{I})^{-1/2}\mathbf{C}^{\mathrm{T}}], \quad \text{where}$$
$$\mathbf{1}_M^{\mathrm{T}} = \underbrace{[1,1,\ldots,1]}_{M\text{ elements}}. \tag{17}$$

The $n \times M$ matrix $\mathbf{S}_j\mathbf{V}^a_{\mathrm{loc}}$ is the modulated LETKF ensemble of analyses at the jth grid column. Note that (11) and (17) utilize the symmetric form $\mathbf{C}(\mathbf{\Gamma}+\mathbf{I})^{-1}\mathbf{C}^{\mathrm{T}}$ of the ETKF discussed by Wang et al. (2004) and Hunt et al. (2007).

Updating entire vertical columns of variables saves as many calls to the ETKF solver as there are vertical model levels [$O(100)$]. However, it also increases the number of observations processed by the ETKF in each call. The net effect of this change to the computational cost will depend on the specific details of the LETKF implementation and the observational network. The number of floating point operations required for the modulated ensemble form of the LETKF depends on the number of observations p within the cylindrical observation volume used to update a vertical column, the number n of model variables in the vertical column being updated, the number of unmodulated ensemble members K, the number of eigenvectors retained when approximating the square root of the vertical localization matrix L, and the number of modulated ensemble members $M = KL$. In current global atmospheric models, we estimate these parameters to have the following orders of magnitude: $p \sim 10^4$, $n \sim 5 \times 10^2$, $K \sim 10^2$, $L \sim 10$, and $M \sim 10^3$. The operation count scaling for the steps required for the ensemble mean update given by (16) is then as follows: $(\tilde{H}_j\mathbf{Z})^{\mathrm{T}}[\mathbf{R}_j^{-1/2}\mathbf{y} - \overline{\tilde{H}_j\mathbf{v}^f}]$ is proportional to $Mp \sim 10^7$ operations while the subsequent operation $[\mathbf{C}(\mathbf{\Gamma}+\mathbf{I})^{-1}\mathbf{C}^{\mathrm{T}}]\{(\tilde{H}_j\mathbf{Z})^{\mathrm{T}}[\mathbf{R}_j^{-1/2}\mathbf{y} - \overline{\tilde{H}_j\mathbf{v}^f}]\}$ is proportional to $M^2 \sim 10^6$ operations and the remaining operations are negligible compared with these results.

The operation count scaling for the ensemble update given by (17) is dominated by the cost of computing $(\mathbf{S}_j\mathbf{Z})[\mathbf{C}(\mathbf{\Gamma}+\mathbf{I})^{-1/2}\mathbf{C}^{\mathrm{T}}]$: a cost that is proportional to $nM^2 \sim 5 \times 10^8$ operations. This cost is smaller than the $M^2p \sim 10^{10}$ cost of forming the $\mathbf{A}$ matrix in (9). However, the $nM^2 \sim 5 \times 10^8$ cost of updating the ensemble mean is comparable with the $M^3 \sim 10^9$ cost of performing the eigenvalue decomposition of (9). Note that there is a strong dependence on the number L of eigenvectors retained from the localization matrix. If only two eigenvectors were retained rather than 10, then the dominant M^2p cost of computing the matrix $\mathbf{A}$ would be reduced by a factor of 25 and if no modulation product was used so that one recovered the basic LETKF, the speed of the procedure would be increased by a factor of 100. A corollary of this fact is that updating 100 vertical grid points simultaneously using a modulated ensemble with $L = 10$ takes 100 times longer than updating a single vertical grid point with no ensemble modulation. However, if there were 100 vertical grid points, the cost of updating the entire vertical column with or without modulation would be about the same.

Within the context of a cycling ensemble data assimilation scheme operating on a computer with sufficient resources to run an ensemble with K members, (17) presents a problem: it gives $M = KL$ posterior ensemble members *but there are only enough computational resources to propagate K members*. How might the K members $\mathbf{X}^a$ be obtained?

A *perturbed observations* approach (Burgers et al. 1998) would be to set

$$\mathbf{S}_j\mathbf{x}^a_{\mathrm{PO},i} = \mathbf{S}_j\mathbf{x}^f_i + (\mathbf{S}_j\mathbf{Z})[\mathbf{C}(\mathbf{\Gamma}+\mathbf{I})^{-1}\mathbf{C}^{\mathrm{T}}] \times (\tilde{H}_j\mathbf{Z})^{\mathrm{T}}[\mathbf{R}_j^{-1/2}(\mathbf{y}+\mathbf{y}'_i) - \tilde{H}_j\mathbf{x}^f_i], \quad i = 1,2,\ldots,K, \tag{18}$$

where $\mathbf{y}'_i$ is the ith vector of K random normally distributed observation perturbations. Each sample of K perturbations has the mean removed so that $\sum_{i=1}^K \mathbf{y}'_i = 0$ and each perturbation is inflated by the factor $\sqrt{K/(K-1)}$ so that $\langle 1/K \sum_{i=1}^K \mathbf{y}'_i\mathbf{y}'^{\mathrm{T}}_i\rangle = \mathbf{R}$. The K analysis states obtained from (18) are stored in the matrix $\mathbf{X}^a_{\mathrm{PO}}$ and the corresponding sample covariance is denoted $\mathbf{P}^a_{\mathrm{PO}}$.

A *stochastic subsampling* approach would be to set

$$\mathbf{S}_j\mathbf{X}^a_{\rm SS} = (\mathbf{S}_j\overline{\mathbf{v}}^a)\mathbf{1}_K^{\rm T} + \mathbf{S}_j\mathbf{Z}^a[\text{randn}(M,K)],$$
$$\text{where}\quad \mathbf{S}_j\mathbf{Z}^a = (\mathbf{S}_j\mathbf{Z})[\mathbf{C}(\mathbf{\Gamma}+\mathbf{I})^{-1/2}\mathbf{C}^{\rm T}] \tag{19}$$

where [randn(M, K)] is an $M \times K$ matrix whose elements are independent random draws from a normal distribution. The sample covariance of the K member ensemble $\mathbf{X}^a_{\rm SS}$ is denoted $\mathbf{P}^a_{\rm SS}$. Note that an appealing aspect to this approach is that the expected covariance of this random sample K-member ensemble is identical to $\mathbf{P}^a_{\rm METKF}$; that is, $\mathbf{P}^a_{\rm METKF} = \langle \mathbf{P}^a_{\rm SS}\rangle$.

A *deterministic subsampling* approach would be to set

$$\mathbf{S}_j\mathbf{X}^a_{\rm DS} = (\mathbf{S}_j\overline{\mathbf{v}}^a)\mathbf{1}_K^{\rm T} + \mathbf{S}_j\mathbf{Z}^a[:,(i{:}\,\delta i{:}\,K\delta i)], \tag{20}$$

where $\mathbf{Z}^a[:,(i{:}\,\delta i{:}\,K\delta i)]$ is the matrix formed by the K columns of $\mathbf{Z}^a$ with indices given by $[i, i+\delta i, i+2\delta i, \ldots, i+K\delta i]$, where the initial index i and the index step δi are tunable parameters. We note that in Kretschmer et al.'s (2015) work using an ensemble expanded by means of augmentation with proxies for climatological forecast errors, a deterministic subsampling approach was used to obtain K initial conditions from an M-member ensemble. In their case, the first K members of the M-member ensemble corresponded to raw forecast perturbations. These were considered better estimates of the true forecast error covariance matrix than the climatological perturbations. To obtain analysis perturbations closely associated with these members, they simply selected the first K members of the posterior ensemble. This is the case of deterministic subselection obtained when one sets $i = \delta i = 1$.

Both of these methods are easy to implement and add little to the cost of the method. In the next section we introduce the GETKF and in the section after that, we present the results of tests that show that the GETKF gives a K-member analysis ensemble covariance matrix $\mathbf{P}^a_{\rm GETKF}$ that is closer to the true analysis error covariance matrix than $\mathbf{P}^a_{\rm PO}$, $\mathbf{P}^a_{\rm SS}$, and $\mathbf{P}^a_{\rm DS}$.

3. The gain form of the ETKF (GETKF)

Note that (11) can be rewritten in the form

$$\begin{aligned}\mathbf{Z}^a &= \mathbf{Z}[\mathbf{C}(\mathbf{\Gamma}+\mathbf{I})^{-1/2}\mathbf{C}^{\rm T}]\\ &= \mathbf{Z} - \mathbf{Z} + \mathbf{Z}[\mathbf{C}(\mathbf{\Gamma}+\mathbf{I})^{-1/2}\mathbf{C}^{\rm T}]\\ &= \mathbf{Z} - \mathbf{Z}[\mathbf{C}\mathbf{C}^{\rm T} - \mathbf{C}(\mathbf{\Gamma}+\mathbf{I})^{-1/2}\mathbf{C}^{\rm T}] \text{ because } \mathbf{C}\mathbf{C}^{\rm T} = \mathbf{I}\\ &= \mathbf{Z} - \mathbf{Z}\mathbf{C}[\mathbf{I} - (\mathbf{\Gamma}+\mathbf{I})^{-1/2}]\mathbf{C}^{\rm T}.\end{aligned} \tag{21}$$

From the last line of (21), we will deduce a form of the ETKF that updates just the K unmodulated perturbations while respecting key aspects of the localized ensemble covariances used by the data assimilation scheme.

Note that the modulated ensemble in observation space $\tilde{H}\mathbf{Z}$ has the concise singular value decomposition (SVD):

$$\tilde{H}\mathbf{Z} = \mathbf{E}\mathbf{\Gamma}^{1/2}\mathbf{C}^{\rm T}. \tag{22}$$

By *concise* SVD, we mean the SVD that removes all of the left and right singular vectors corresponding to zero singular values. Equation (22) implies that

$$\mathbf{E} = \tilde{H}\mathbf{Z}\mathbf{C}\mathbf{\Gamma}^{-1/2} \text{ and that } \mathbf{C}^{\rm T} = \mathbf{\Gamma}^{-1/2}\mathbf{E}^{\rm T}\tilde{H}\mathbf{Z}. \tag{23}$$

Using (23) in (21) gives

$$\mathbf{Z}^a = \mathbf{Z} - \{\mathbf{Z}\mathbf{C}[\mathbf{I} - (\mathbf{\Gamma}+\mathbf{I})^{-1/2}]\mathbf{\Gamma}^{-1}\mathbf{C}^{\rm T}(\tilde{H}\mathbf{Z})^{\rm T}\}(\tilde{H}\mathbf{Z}). \tag{24}$$

Like (11), (24) yields $M = KL$ posterior perturbations. However, note that (24) can be approximated by

$$\begin{aligned}&\mathbf{Z}^a \cong [\mathbf{I} - \{\mathbf{Z}\mathbf{C}[\mathbf{I} - (\mathbf{\Gamma}+\mathbf{I})^{-1/2}]\mathbf{\Gamma}^{-1}\mathbf{C}^{\rm T}(\tilde{H}\mathbf{Z})^{\rm T}\}\tilde{\mathbf{H}}]\mathbf{Z}, \quad \text{where}\\ &\tilde{\mathbf{H}} = \mathbf{R}^{-1/2}\frac{\partial H(\overline{\mathbf{x}}^f)}{\partial(\overline{\mathbf{x}}^f)^{\rm T}}\\ &\quad = (\mathbf{I} - \tilde{\mathbf{K}}\tilde{\mathbf{H}})\mathbf{Z} = (\mathbf{I} - \tilde{\mathbf{K}}\tilde{\mathbf{H}})\left[\frac{\mathbf{V}^f - \overline{\mathbf{v}}^f\mathbf{1}_M^{\rm T}}{\sqrt{M}}\right] = \left[\frac{\mathbf{V}^a_{\rm loc} - \overline{\mathbf{v}}^a\mathbf{1}_M^{\rm T}}{\sqrt{M}}\right],\end{aligned} \tag{25}$$

where $\tilde{\mathbf{K}} = \{\mathbf{Z}\mathbf{C}[\mathbf{I} - (\mathbf{\Gamma}+\mathbf{I})^{-1/2}]\mathbf{\Gamma}^{-1}\mathbf{C}^{\rm T}(\tilde{H}\mathbf{Z})^{\rm T}\}$ is the GETKF counterpart of the modified Kalman gain[1] appropriate for ensemble perturbations discussed in Whitaker and Hamill (2002) and $\tilde{\mathbf{H}}$ is the observation operator linearized mean and normalized by the inverse square root of the observation error covariance matrix. The form of (25) suggests that we could replace the modulated ensemble perturbations $[(\mathbf{v}_i^f - \overline{\mathbf{v}}^f\mathbf{1}_M^{\rm T})/\sqrt{M}]$ that the matrix $(\mathbf{I} - \tilde{\mathbf{K}}\tilde{\mathbf{H}})$ left multiplies by $[\mathbf{x}_i^f - \overline{\mathbf{x}}^f]$ the raw unmodulated K ensemble perturbations. Doing so yields an equation for the ith posterior ensemble member of the form

$$[\mathbf{x}_i^a - \overline{\mathbf{x}}^a] = [\mathbf{x}_i^f - \overline{\mathbf{x}}^f] - \tilde{\mathbf{K}}\tilde{\mathbf{H}}[\mathbf{x}_i^f - \overline{\mathbf{x}}^f], \quad i = 1,2,\ldots,K, \tag{26}$$

where the posterior analysis mean $\overline{\mathbf{x}}^a$ has been set equal to the $\overline{\mathbf{v}}^a$ obtained from (12). Equation (26) associates an analysis member $\mathbf{x}_i^a$ to each raw, unmodulated forecast member $\mathbf{x}_i^f$. For the single observation case ($p = 1$), it

[1] The modified gain discussed here is to map prior ensemble perturbations to posterior perturbations. In contrast, the modified gains of Penny (2014), Hamrud et al. (2015), and Bonavita et al. (2015) map prior means to posterior means.

can be shown that (26) would give identical results to Whitaker and Hamill's (2002) and Anderson's (2001) filters.

Note that a key step in obtaining (26) was to simply replace $[(\mathbf{v}_i^f - \overline{\mathbf{v}}^f\mathbf{1}_M^{\mathrm{T}})/\sqrt{M}]$ by $[\mathbf{x}_i^f - \overline{\mathbf{x}}^f]$ in (25). Making the corresponding replacements in (24) and skipping the linearization step of (25) gives

$$\mathbf{x}_i^a = \overline{\mathbf{x}}^a + \left\{(\mathbf{x}_i^f - \overline{\mathbf{x}}^f) - \mathbf{Z}\mathbf{C}[\mathbf{I} - (\mathbf{\Gamma} + \mathbf{I})^{-1/2}]\mathbf{\Gamma}^{-1}\mathbf{C}^{\mathrm{T}} \times (\tilde{H}\mathbf{Z})^{\mathrm{T}}\left[\tilde{H}(\mathbf{x}_i^f) - \frac{1}{K}\sum_{i=1}^{K}\tilde{H}(\mathbf{x}_i^f)\right]\right\}, \tag{27}$$

for $i = 1, 2, \ldots, K$. Unlike (26), (27) was derived without linearizing the observation operator and hence does not have explicit dependence on the degree of linearity of the observation operator.

Within the context of an LETKF, the assimilated observations would be confined to some observation volume and (27) would only update a single vertical column near the center of the observation volume. In this case, (27) is better expressed as

$$\mathbf{S}_j\mathbf{x}_i^a = \mathbf{S}_j\overline{\mathbf{x}}^a + \mathbf{S}_j\{(\mathbf{x}_i^f - \overline{\mathbf{x}}_i^f) - \mathbf{Z}\mathbf{C}[\mathbf{I} - (\mathbf{\Gamma} + \mathbf{I})^{-1/2}]\mathbf{\Gamma}^{-1}\mathbf{C}^{\mathrm{T}} \times (\tilde{H}_j\mathbf{Z})^{\mathrm{T}}\mathbf{R}_j^{-1/2}[H_j(\mathbf{x}_i^f) - \overline{H_j(\mathbf{x}^f)}]\}, \quad \text{where}$$
$$\overline{H_j(\mathbf{x}^f)} = \frac{1}{K}\sum_{i=1}^{K}H_j(\mathbf{x}_i^f). \tag{28}$$

Thus, (28) allows the analysis perturbations corresponding to the forecast perturbations to be obtained in a way that is consistent with the localized ensemble covariances. To better reflect on the way (28) determines ensemble perturbations and to allow for the inclusion of a posterior initial perturbation inflation/attenuation factor, it is helpful to rewrite it in terms of an expression for the $n \times K$ matrix $\mathbf{X}^a$ of analysis members:

$$\mathbf{S}_j\mathbf{X}^a = (\mathbf{S}_j\overline{\mathbf{x}}^a)\mathbf{1}_K^{\mathrm{T}} + a\{\mathbf{S}_j\mathbf{X}^{f\prime} - \mathbf{S}_j\mathbf{Z}\mathbf{C}[\mathbf{I} - (\mathbf{\Gamma} + \mathbf{I})^{-1/2}]\mathbf{\Gamma}^{-1}\mathbf{C}^{\mathrm{T}} \times (\tilde{H}\mathbf{Z})^{\mathrm{T}}(\tilde{H}\mathbf{X}^{f\prime})\} = (\mathbf{S}_j\overline{\mathbf{x}}^a)\mathbf{1}_K^{\mathrm{T}} + a(\mathbf{S}_j\mathbf{X}_{\mathrm{raw}}^{a\prime}), \tag{29}$$

where $(\mathbf{S}_j\mathbf{X}_{\mathrm{raw}}^{a\prime})$ is a raw estimate of the analysis perturbations to be added to the analysis mean to create the new ensemble. [Note that the matrix $(\mathbf{S}_j\mathbf{X}_{\mathrm{raw}}^{a\prime})$ is precisely equal to the term in curly brackets in (29).]

Equation (29) contains two distinct proxies for forecast error realizations: the M-member modulated ensemble $\mathbf{Z}$ and the K forecast ensemble perturbations $\mathbf{X}^{f\prime}$ produced by the nonlinear model. The former has a relatively high-rank covariance matrix; the latter a lower rank covariance matrix. As discussed by Wang et al. (2007), the ETKF systematically underestimates the analysis error variance when the rank of the ensemble covariance matrix in observation space $\tilde{H}\mathbf{P}_{\mathrm{ens}}^f\tilde{H}^{\mathrm{T}}$ is significantly lower than the rank of the corresponding true covariance matrix $\tilde{H}\mathbf{P}\tilde{H}^{\mathrm{T}}$. Given the similarity of the GETKF to the ETKF, we should anticipate that (29) is likely to provide a poorer estimate of the average analysis error variance than (10). To ensure that this deficiency does not affect the variance of the GETKF perturbations generated by (29), we denote $\mathbf{S}_j\mathbf{P}_{\mathrm{raw}}^a\mathbf{S}_j^{\mathrm{T}} = (\mathbf{S}_j\mathbf{X}_{\mathrm{raw}}^{a\prime})(\mathbf{S}_j\mathbf{X}_{\mathrm{raw}}^{a\prime})^{\mathrm{T}}/(K-1)$ and set

$$a = \sqrt{\frac{[\mathrm{trace}(\mathbf{S}_j\mathbf{P}_{\mathrm{METKF}}^a\mathbf{S}_j^{\mathrm{T}})]}{\mathrm{trace}(\mathbf{S}_j\mathbf{P}_{\mathrm{raw}}^a\mathbf{S}_j^{\mathrm{T}})}}, \tag{30}$$

in (29). Note that this inflation factor can be computed before observations are assimilated, and it is not directly related to the size of the difference between the observations and forecasts. We shall simply refer to it as *inherent GETKF inflation*. This factor ensures that the average analysis error variance produced by the GETKF is identical to that produced by the METKF. We shall denote the covariance matrix of the analysis ensemble obtained using (30) in (29) by $\mathbf{P}_{\mathrm{GETKF}}^a$.

To better understand the properties of $\mathbf{P}_{\mathrm{GETKF}}^a$, it is useful to consider the expected value of $\mathbf{P}_{\mathrm{GETKF}}^a$ in the case of a linear observation operator:

$$\mathbf{S}_j[\mathbf{x}_i^a - \overline{\mathbf{x}}^a] = a\mathbf{S}_j\{[\mathbf{x}_i^f - \overline{\mathbf{x}}^f] - \tilde{\mathbf{K}}\tilde{\mathbf{H}}[\mathbf{x}_i^f - \overline{\mathbf{x}}^f]\}, \text{ and hence}$$
$$\mathbf{S}_j\langle\mathbf{P}_{\mathrm{GETKF}}^a\rangle\mathbf{S}_j^{\mathrm{T}} = a^2\mathbf{S}_j\{\mathbf{P} - \tilde{\mathbf{K}}\tilde{\mathbf{H}}\mathbf{P} - \mathbf{P}\tilde{\mathbf{H}}^{\mathrm{T}}\tilde{\mathbf{K}}^{\mathrm{T}} + \tilde{\mathbf{K}}\tilde{\mathbf{H}}\mathbf{P}\tilde{\mathbf{H}}^{\mathrm{T}}\tilde{\mathbf{K}}^{\mathrm{T}}\}\mathbf{S}_j^{\mathrm{T}}. \tag{31}$$

For future reference, we will denote $\langle\mathbf{P}_{\mathrm{GETKF}}^a\rangle$ by $\mathbf{P}_{\mathrm{GOPT}}^a$.

With (29), the number of operations required to update an individual ensemble member is roughly the same as updating the ensemble mean [see (12)]. This means that the dominant computational cost is proportional to $Mp \sim 10^7$ for each ensemble member update. With $K \sim 100$, this gives a total cost proportional to $KMp \sim 10^9$ for updating the entire ensemble. This is slightly larger than the order $nM^2 \sim 5 \times 10^8$ operations associated with the standard ETKF ensemble update. However, it is still smaller than the $M^2p \sim 10^{10}$ operation factor associated with computing the $\mathbf{A}$ matrix of

(9). The $M^2p \sim 10^{10}$ cost is also much larger than that associated with computing the inflation factor in (30). Thus, we anticipate that the overall cost of updating the ensemble using (29) will be similar to that associated with the METKF update given by (17).

4. Comparison of the accuracy of $\mathbf{P}^a_{\mathrm{GETKF}}$ with $\mathbf{P}^a_{\mathrm{PO}}$, $\mathbf{P}^a_{\mathrm{SS}}$, and $\mathbf{P}^a_{\mathrm{DS}}$ in a simple model

Within the context of the simple statistical model discussed earlier, our observation volume and the set of variables to be updated are identical, so we can drop the selection operator from (29). As shown in the appendix, the true analysis error covariance matrix $\mathbf{P}^a = \langle \boldsymbol{\varepsilon}^a (\boldsymbol{\varepsilon}^a)^{\mathrm{T}} \rangle$ associated with the METKF analysis mean is given by

$$\mathbf{P}^a = \mathbf{P} - \mathbf{K}\tilde{H}\mathbf{P} - (\mathbf{K}\tilde{H}\mathbf{P})^{\mathrm{T}} + \mathbf{K}[\tilde{H}\mathbf{P}\tilde{H}^{\mathrm{T}} + \mathbf{I}]\mathbf{K}^{\mathrm{T}},$$
$$\text{where} \quad \mathbf{P} = \langle \boldsymbol{\varepsilon}^f (\boldsymbol{\varepsilon}^f)^{\mathrm{T}} \rangle, \tilde{H}\mathbf{P} = \langle \tilde{H}\boldsymbol{\varepsilon}^f (\boldsymbol{\varepsilon}^f)^{\mathrm{T}} \rangle, \quad \text{and}$$
$$\tilde{H}\mathbf{P}\tilde{H}^{\mathrm{T}} = \langle \tilde{H}\boldsymbol{\varepsilon}^f (\tilde{H}\boldsymbol{\varepsilon}^f)^{\mathrm{T}} \rangle, \tag{32}$$

where $\mathbf{K} = \mathbf{Z}^a (\tilde{H}\mathbf{Z}^a)^{\mathrm{T}}$ is the METKF gain matrix used to obtain the METKF posterior mean using (12). In our simple statistical model, the true forecast error covariance matrices $\mathbf{P}$, $\mathbf{P}\tilde{H}^{\mathrm{T}}$ and $\tilde{H}\mathbf{P}\tilde{H}^{\mathrm{T}}$ are precisely known, so it is a simple matter to compute the true analysis error covariance matrix $\mathbf{P}^a$ associated with the ensemble-based METKF suboptimal gain. This enables us to use $\mathbf{P}^a$ to measure the inaccuracy of the K-member analysis ensemble covariance matrices $\mathbf{P}^a_{\mathrm{PO}}$, $\mathbf{P}^a_{\mathrm{SS}}$, $\mathbf{P}^a_{\mathrm{DS}}$, and $\mathbf{P}^a_{\mathrm{GETKF}}$, respectively, corresponding to the perturbed observations (18), stochastic subsampling (19), deterministic subsampling (20), and the GETKF (29) approaches. It is also of interest to measure the error of the statistically expected analysis error covariance matrices $\langle \mathbf{P}^a_{\mathrm{SS}} \rangle = \mathbf{P}^a_{\mathrm{METKF}}$ (10) and $\langle \mathbf{P}^a_{\mathrm{GETKF}} \rangle = \mathbf{P}^a_{\mathrm{GOPT}}$ (31).

The similarity of all these approximate analysis error covariance matrices to the true analysis error covariance matrix $\mathbf{P}^a$ was measured with two distinct measures. First, we compute the weighted mean square error of each of the elements given by

$$\mathrm{mse}(\mathbf{P}^a_{\mathrm{approx}}) = \frac{1}{n^2} \sum_{j=1}^{n} \sum_{i=1}^{n} \{\mathbf{F}\}_{ij} (\{\mathbf{P}^a_{\mathrm{approx}}\}_{ij} - \{\mathbf{P}^a\}_{ij})^2, \tag{33}$$

where $\mathbf{P}^a_{\mathrm{approx}}$ is some approximation to the true analysis error covariance matrix $\mathbf{P}^a$ obtained from (32) and the weighting $\{\mathbf{F}\}_{ij}$ is given by the (ij)th element of the localization matrix $\mathbf{F}$. Such weighting is justifiable because sampling errors are unavoidable away from the diagonal, and during data assimilation, such sampling errors are attenuated by a localization matrix. The second measure we employ is that of the unweighted "correlation" of the elements given by

$$\mathrm{corr}(\mathbf{P}^a_{\mathrm{approx}}) = \frac{\sum_{j=1}^{n} \sum_{i=1}^{n} (\{\mathbf{P}^a_{\mathrm{approx}}\}_{ij} \{\mathbf{P}^a\}_{ij})}{\sqrt{\sum_{j=1}^{n} \sum_{i=1}^{n} (\{\mathbf{P}^a\}_{ij})^2} \sqrt{\sum_{j=1}^{n} \sum_{i=1}^{n} (\{\mathbf{P}^a_{\mathrm{approx}}\}_{ij})^2}}. \tag{34}$$

Note that $\mathrm{corr}(\mathbf{P}^a_{\mathrm{approx}}) = 1$ if $\mathbf{P}^a_{\mathrm{approx}} = b\mathbf{P}^a$, where b is some arbitrary scalar. Thus, (34) may be viewed as a measure of the similarity of the shapes of the two covariance matrices as it is independent of the amplitude of the field while (33) measures some combination of the similarity of shape and amplitude. In considering (34), note that since $\{\mathbf{P}^a\}_{ij}$ is near zero for distant variables, in the product $(\{\mathbf{P}^a_{\mathrm{approx}}\}_{ij} \{\mathbf{P}^a\}_{ij})$ the corresponding (possibly spurious) analysis ensemble correlations $\{\mathbf{P}^a_{\mathrm{approx}}\}_{ij}$ between distant variables are not able to affect the measure $\mathrm{corr}(\mathbf{P}^a_{\mathrm{approx}})$.

The MSE and correlation measures of accuracy were computed over eight entirely independent trials. Figure 5 plots the MSE and correlation measures over each of these trials for $\mathbf{P}^a_{\mathrm{PO}}$ (green line), $\mathbf{P}^a_{\mathrm{SS}}$ (blue line), $\mathbf{P}^a_{\mathrm{GETKF}}$ (black line), $\mathbf{P}^a_{\mathrm{METKF}}$ (mauve line), and $\mathbf{P}^a_{\mathrm{GOPT}}$ (red line). It shows that in each of these trials, under both the MSE and correlation measures of accuracy, the

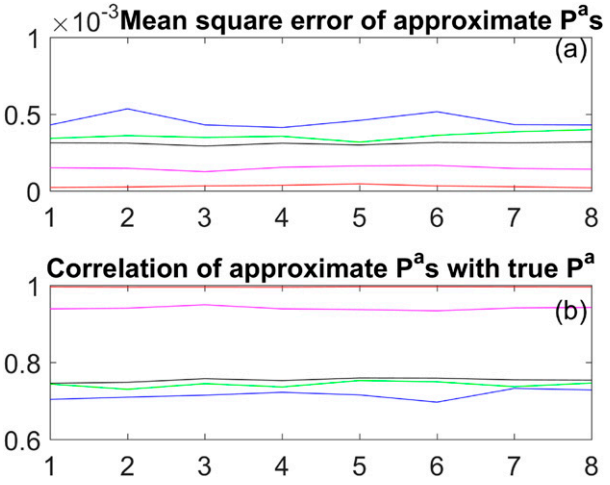

FIG. 5. (a) The weighted MSE [see (33)] of estimates of the true analysis error covariance matrix $\mathbf{P}^a$ associated with $\mathbf{P}^a_{\mathrm{PO}}$ (green line), $\mathbf{P}^a_{\mathrm{SS}}$ (blue line), $\mathbf{P}^a_{\mathrm{GETKF}}$ (black line), $\mathbf{P}^a_{\mathrm{METKF}}$ (mauve line), and $\mathbf{P}^a_{\mathrm{GOPT}}$ (red line) for eight entirely independent trials. (b) As in (a), but for lines that pertain to the correlation [see (34)] between the approximate and true elements of the analysis error covariance matrix.

ranking from the most accurate to the least accurate estimate of the analysis error covariance matrix was as follows: $\mathbf{P}^a_{\mathrm{GOPT}}$, $\mathbf{P}^a_{\mathrm{METKF}}$, $\mathbf{P}^a_{\mathrm{GETKF}}$, $\mathbf{P}^a_{\mathrm{PO}}$, and $\mathbf{P}^a_{\mathrm{SS}}$.

We have not displayed the results for the deterministic subsampling technique in Fig. 5 because it was found that $\mathbf{P}^a_{\mathrm{DS}}$ gave worse results than all of the other methods. As good a $\mathbf{P}^a_{\mathrm{DS}}$ as any other was obtained from setting $\mathbf{X}^a_{\mathrm{DS}} = (\mathbf{S}_j\bar{\mathbf{v}}^a)\mathbf{1}^{\mathrm{T}}_K + \mathbf{S}_j\mathbf{Z}^a[:, \{1{:}\,L-1{:}\,K(L-1)\}]$. Recalling that $K = 50$ and $L = 10$ in our simple model experiment, this approach selects six members (1, 10, 19, 28, 37, and 46) that are raw members modulated by column 1 of the truncated renormalized localization matrix and six more members (55, 64, 73, 82, 91, and 100) that are raw members modulated by column 2, and so on until 50 members were obtained. There was not a great deal of sensitivity to changing which modulated ensemble members were selected. The deterministic selection procedure associated with the above equation was found to be better than or statistically indistinguishable from other selection procedures. In this case, this selection procedure was significantly superior to that used by Kretschmer et al. (2015) of just choosing the first 50 members of the expanded ensemble, which correspond to the 50 raw members modulated by column 1 of the localization matrix. However, since the ensemble expansion technique employed by Kretschmer et al. (augmentation with climatological forecast error proxies) is very different from the ensemble modulation expansion technique used here, our result does not imply that Kretchmer et al.'s deterministic subselection approach was suboptimal for their application.

Most promising for the GETKF is the fact that its analysis ensemble covariance matrix estimate was *always* closer to the true forecast error covariance matrix than any of the other techniques of obtaining K analysis perturbations from the M METKF analysis perturbations.

5. Cycling experiments with a simple dynamical model

To further examine GETKF performance, here we test it in a data assimilation cycling mode using a newly created "storm track" version of the Lorenz-96 model (Lorenz and Emanuel 1998) and observations that are an integral of the state.

The storm-track model differs from the Lorenz and Emanuel (1998) model in three ways; 1) it uses 80 grid points instead of 40, 2) the linear damping term $-x_j$ is replaced by $-[0.5 + 2\cos^4(j\pi/80)]x_j$, and 3) the forcing term F (which is set to a constant value of 8 in the original model) is treated as an independent random variable at every grid point. Specifically, if the forcing at the previous time step was F_{old}, then the equation used to compute the forcing at the new time step F_{new} is given by

$$F_{\mathrm{new}} = rF_{\mathrm{old}} + (1-r)G, \tag{35}$$

where G is a random number drawn from a gamma distribution. To interpret the scalar r in this equation, note that right multiplying (35) by F_{old} and recalling that, by construction $\langle GF_{\mathrm{old}}\rangle = 0$ and $\langle F^2_{\mathrm{old}}\rangle = \langle F^2_{\mathrm{new}}\rangle$, it follows that $r = \langle F_{\mathrm{new}}F_{\mathrm{old}}\rangle / \sqrt{\langle F^2_{\mathrm{old}}\rangle\langle F^2_{\mathrm{new}}\rangle}$ gives the correlation of F over one time step. We set $r = e^{-1/3}$ consistent with an e-folding time scale of three model time steps.

Equation (35) also implies that

$$\begin{aligned}\langle F\rangle &= r\langle F\rangle + (1-r)\langle G\rangle, \text{ because } \langle F_{\mathrm{new}}\rangle = \langle F_{\mathrm{old}}\rangle \\ &= \langle F\rangle \Rightarrow \langle F\rangle = \langle G\rangle,\end{aligned} \tag{36}$$

where the angle brackets indicate the expectation operator. Hence, (36) implies that the mean of the F values produced by (35) must equal the mean of G. We set the mean of the gamma distribution from which the values of G to be equal to 8, thus ensuring that $\langle F\rangle = 8$.

Subtracting the mean from both sides of (35), and then squaring and taking expectations, leads to

$$\mathrm{var}(G) = \frac{(1+r)}{(1-r)}\mathrm{var}(F). \tag{37}$$

We chose to set $\mathrm{var}(G) = [(1+r)/(1-r)](1/8)$, thus ensuring that the variance of the random time series of F about its mean value of 8 was equal to 1/8.

The spatially varying linear damping term $-[0.5 + 2\cos^4(j\pi/80)]x_j$ results in a damping that is 2.5 times the nominal value at each end of the periodic domain, decreasing to half the nominal value in the middle. Figure 6 shows that these changes lend a storm-track-like pattern of behavior to the Lorenz-96 model, and for this reason we refer to it as a storm-track version of the model. The climatological covariance matrix (Fig. 7) for this model shows that covariances between state variables, though weaker, are more coherent in space in the high-damping regions at either end of the periodic domain. The statistical properties of the random forcing are identical in the truth run and the forecast model, but different random seeds are used so that the random sequences are different. The random forcing introduces a small-scale and irreducible source of random error covariance to the true background-error covariance in the ensemble data assimilation (in addition to sampling error) that cannot be reduced by, for example, increasing ensemble size. As a consequence, the analysis error asymptotes to a higher minimum level, as the ensemble size and localization length scale are increased. For the purposes of this paper, this is desirable because the differences

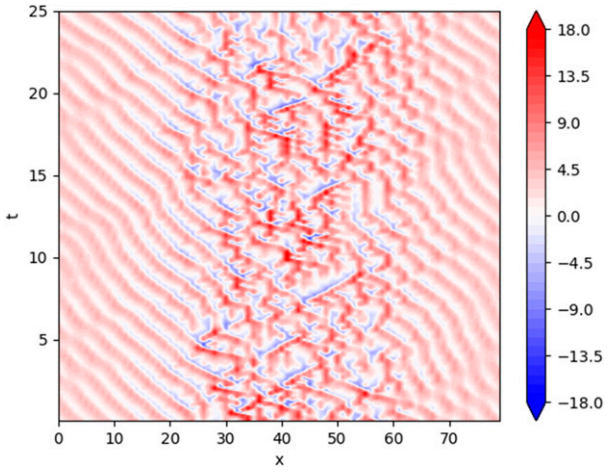

FIG. 6. Contours as a function of time (y axis) and space (x axis) for the modified version of the Lorenz-96 model described in section 5 with zonally varying damping and random forcing. Note that the solution is low amplitude and fairly regular in the high-damping regions at either end of the periodic domain, and high amplitude and chaotic in the center of the domain where the damping is 5 times weaker.

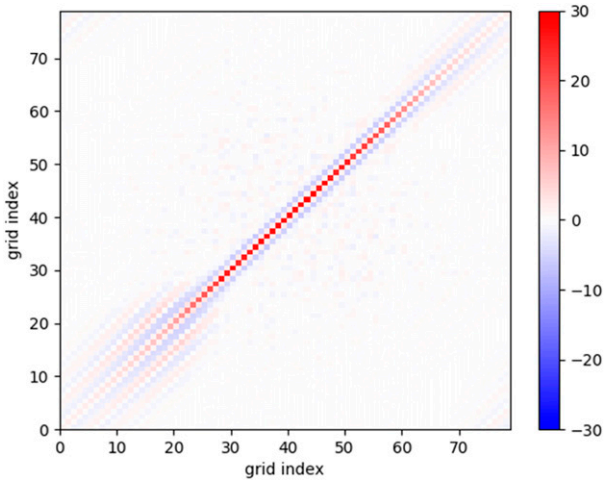

FIG. 7. The climatological covariance matrix for the modified Lorenz model.

between the assimilation algorithms are most evident at smaller localization scales and disappear entirely at long localization scales.

Data assimilation experiments are performed with eight ensemble members, using the serial algorithm of Whitaker and Hamill (2002) (incorporating both observation space localization and model space localization via modulated ensembles), the METKF and the GETKF (both of which employ model space localization using modulated ensembles). All experiments use the observation-dependent posterior inflation algorithm of Hodyss et al. (2016).[2] The tunable parameters for the inflation scheme [a and b in Eq. (4.4) of Hodyss et al. (2016)] are both fixed to 1.0 for all of the experiments. Note that for the GETKF, the Hodyss et al. posterior inflation is applied to the perturbations obtained using (29), where (29) includes the multiplicative factor a that through (30) ensures that the trace of the GETKF posterior covariance matrix is identical to that of the corresponding METKF posterior covariance.

Each observed value is equal to the average of seven spatially contiguous grid points. Each grid point has a unique average associated with it. Anderson and Lei (2013) found that such *integral* observations are particularly challenging for observation space localization in the standard 40-variable Lorenz-96 model. These observations are analogous to satellite radiance observations, where the forward radiative transfer operator involves a vertical integral of the state.[3]

Since we chose to assimilate all 80 unique seven-point running averages of the system each data assimilation cycle, the observation error covariance matrix **R** has the same size as the forecast error covariance matrix **P**. We assumed **R** to be diagonal with diagonal elements equal to 0.01. Observations are assimilated every time step (6 h or 0.05 nondimensional time units) and experiments are run for 100 000 assimilation cycles after a spinup period of 1000 assimilation cycles, with both observation space and model space localization.

When using idealized models for data assimilation experiments, it is of interest to note the ratio of the error-doubling time to the data assimilation time interval. While we have not performed a detailed analysis of the error-doubling time in this model, we do know how our modifications to the original Lorenz and Emanuel (1998) model alter the growth of ensemble spread. Specifically, allowing the diffusion to vary zonally had little overall impact on the growth of the ensemble spread but changing the forcing F from a constant to a randomly varying F increased the growth of the spread over a single time step from 1.15 to 1.66. This suggests that the error-doubling time for our modified version of this model is even shorter than that of the original model. Lorenz and Emanuel (1998) state that the error-doubling time of their original model was 2 days—8 times larger than the data assimilation time

[2] Code in the Python programming language to reproduce all of the experiments shown here is available online (https://github.com/jswhit/L96).

[3] Many radiance observations are vertical integrals of nonlinear functions of the state but, for simplicity, we ignore such complexities in this paper.

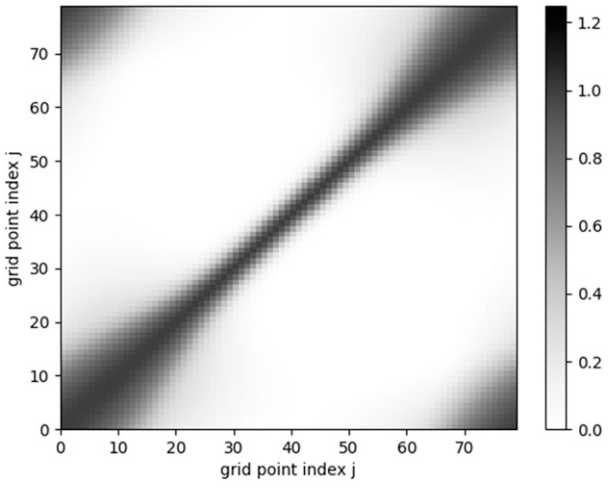

FIG. 8. Covariance localization matrix implied by (39) with $d_0 = 20$.

interval used in our experiments so it would be less than 8 times larger in our experiments.

Both observation space and model space localization use a Gaspari–Cohn (GC) function (Gaspari and Cohn 1999). We denote the GC function by GC(d_{ij}, l). Here, GC(d_{ij}, l) is a function of the separation distance d_{ij} between the ith and jth grid points and a length scale l. The structure of the climatological covariance matrix (Fig. 7) suggests that a spatially varying covariance localization length scale, tighter in the center of the domain and broader at each end, should perform better than a constant localization scale. The variation of the covariance function length scale appears to mirror the spatial structure of the linear damping terms; furthermore, dynamical reasoning suggests that error correlation length scales would also be partially controlled by the linear damping term. For those two reasons, and to reduce the size of the parameter space of varying localization length scales to be explored, we chose to let the GC localization length scale have the same spatial structure as the linear damping term so that

$$l = l(m) = [0.5 + 2\cos^4(m\pi/80)]d_0, \qquad (38)$$

where m is the index locating the grid point of interest and d_0 is a reference localization length scale. To create a symmetric localization matrix from the GC function, we let the (ij)th element of this localization matrix $\mathbf{F}$ be given by

$$\{\mathbf{F}\}_{ij} = \frac{1}{2}\{\mathrm{GC}[d_{ij}, l(i)] + \mathrm{GC}[d_{ji}, l(j)]\}. \qquad (39)$$

Note that the blending of the GC functions associated with the ith and jth grid points in (39) ensures that the localization matrix is symmetric. We have confirmed that the use of the spatially varying length scale given by (38) results in analysis errors that are about 10% smaller than any constant localization length scale. A plot of the localization matrix arising from (39) is given in Fig. 8 for the case where the reference localization length scale $d_0 = 20$.

In our implementation of the observation space localization form of the serial EnSRF, each observation is used to update the mean and K raw perturbations of the state variables using ensemble covariances localized with the function given by (39) in which the distance d_{ij} between the observation and a state variable is computed by assuming that the observation is located at the middle of the kth boxcar averaging kernel. In other words, the "location" assigned to each observation is the fourth grid point of the seven consecutive grid points involved in the running average that defines the observation.

For model space localization, a synthetic modulation product ensemble is created by modulating the eight-member ensemble with the eigenvectors of the localization matrix implied by the spatially varying GC localization function using the procedure described in section 2. In all experiments, we ensure that the number L of leading eigenvectors retained in our approximation of (39)'s localization matrix is sufficient to explain 99% of the trace of **F.** The scaled eigenvectors are then used to perform the modulation, leading to a synthetic ensemble of size $8L$, where L is a function of the reference localization length scale d_0 [see (38)] of the GC function. As d_0 decreases, L increases. When the modulated ensemble is used in the serial EnSRF, each observation and the modulated ensemble covariances are used to update the mean, the M modulated perturbations, and the K raw perturbations of the state variables. The modulated ensemble covariances are not localized because the localization is already "baked into" the ensemble via the modulation product. After all observations have been assimilated by the serial EnSRF, the fully updated K raw perturbations are added back to the posterior mean to create the final posterior ensemble and this K member ensemble is propagated forward by the nonlinear model.

The GETKF simultaneously assimilates all of the observations in the local observation volume, using (12) to update the ensemble mean and (29) to update the K raw ensemble perturbations. In this toy model example, the local observation volume is global in that it contains *all* of the observations.

The METKF, on the other hand, involves the computation of a set of weights that are used to transform the entire set of $8L$-member background ensemble perturbations into an $8L$-member set of analysis

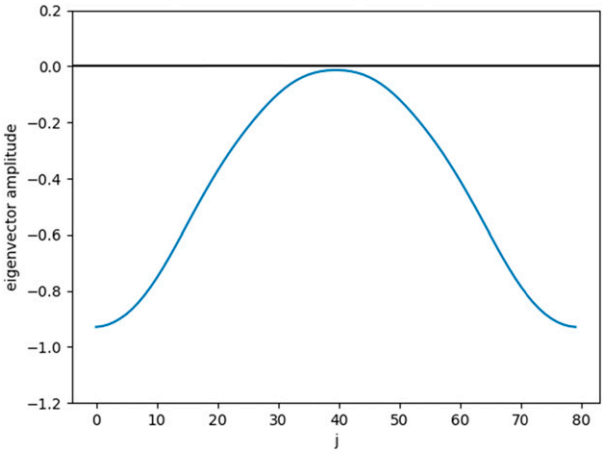

FIG. 9. First eigenvector of localization matrix shown in Fig. 8.

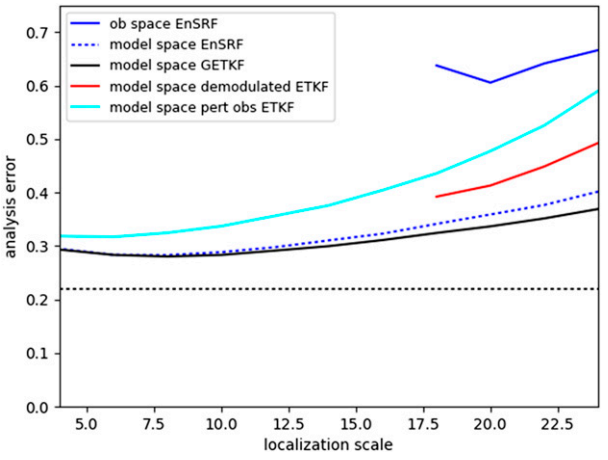

FIG. 10. RMSE as a function of the reference GC localization length scale d_0. Results for the serial EnSRF for observation space localization and model space localization are shown by the solid and dashed blue lines, respectively. Results for the demodulated METKF and GETKF with model space localization are shown by the red and black lines, respectively. Results for the perturbed-obs METKF are shown in cyan. For reference, the horizontal black dashed line shows the RMSE obtained with a 256-member ETKF with no horizontal localization.

ensemble perturbations. The first eight members of the *prior* $8L$-member modulated ensemble are in fact the original eight members propagated by the forecast model multiplied by the first eigenvector of the localization matrix. This knowledge suggests an ad hoc approach in which one would try and "undo" the modulation in the posterior ensemble by elementwise dividing each of the first eight members of the posterior ensemble by the first eigenvector of the localization matrix. Since the first eigenvector typically has a relatively simple structure without zero values, demodulation of the first eight posterior members by the first eigenvector seems like the best option. We call this approach the "demodulated" METKF.

Figure 9 shows the structure of the first eigenvector of the localization matrix with $d_0 = 20$. Since the amplitude of the eigenvector changes by a factor of 68 across the domain, undoing the modulation by dividing the posterior ensemble perturbations by this eigenvector results in a loss of roughly two decimal places of precision. The amount of precision lost is a function of the severity of the localization, as using $d_0 = 10$ (15) instead of 20 results in a loss of 9 (5) digits of precision. We note in the case of the operational NCEP data assimilation system that the first eigenvector of the vertical localization matrix contains values very close to zero, and these near-zero values cause an extreme loss of precision in the updated ensemble, so that the demodulated METKF approach is infeasible. For the same reason, the demodulated METKF approach was also unworkable for the set of problems considered in section 4. As previously noted, another alternative is to use the perturbed observations approach [see (18)].

Figure 10 shows the root-mean-square error (RMSE) of the ensemble mean analysis (relative to the nature run used to generate the observations) for the serial filter using observation space localization, the METKF (both the "perturbed-obs" and demodulated variants) and the GETKF using model space localization, as a function of the GC localization length scale d_0. For reference, the horizontal black dashed line shows the near-optimal analysis error obtained by running a 256-member ETKF with no localization. For all values of d_0, model space localization outperforms observation space localization. The GETKF outperforms the demodulated METKF for the d_0 values for which the demodulated METKF is stable. The demodulated METKF fails for $d_0 < 18$. The demodulated METKF outperforms the perturbed-obs variant for localization length scales at which it is stable, but the perturbed-obs METKF is stable for all d_0 localization scales, and has a lower minimum error. Deterministic or stochastic subsampling can also be used within the METKF to choose a subset of ensemble perturbations to advance to the next observation time, as discussed in section 4. Both of these subsampling approaches were found to perform poorly in cycled data assimilation mode with this simple system.

The modulated-ensemble serial filter with model space localization performs identically to the GETKF when the adjustment factor a in (29) is set equal to 1. However, when (30) is used to define a, the GETKF outperforms the modulated-ensemble serial filter for $d_0 > 10$ and is about the same or marginally better than the serial filter for $d_0 \leq 10$.

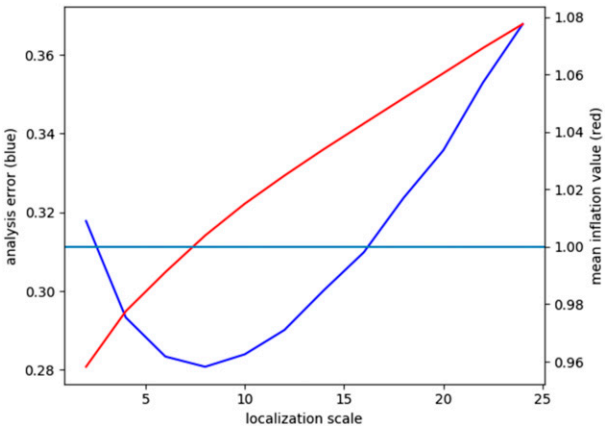

FIG. 11. The ordinate axis on the right pertains to the mean GETKF inflation value a from (33). The red line shows how this value changes with localization scale. The ordinate axis on the left refers to the analysis error of the GETKF and the blue line shows how this changes with localization length scale. (Although the vertical scale is different, this line is identical to the black line in Fig. 10.) Interestingly, the a value is approximately equal to 1 at the same localization length scale that minimizes the analysis error.

Figure 11 shows that when (30) is used to define a, its average value increases with increasing localization length scale d_0. Intriguingly, at the localization length scale that minimizes RMSE, a is approximately equal to 1 and has a neutral or small effect on ensemble perturbation size. If it were generally true that the localization that makes the inherent GETKF inflation neutral also minimizes RMSE, one could adaptively decide the vertical localization for each vertical column by varying the localization until the "a" obtained from (30) became equal to 1. We leave it to future research to assess the merit of the associated hypothesis that *the localization that neutralizes inherent GETKF inflation also minimizes RMSE.*

6. Conclusions

The GETKF has been introduced and described. It is a variation on the ETKF that provides a solution to the problem of how to rapidly obtain just K posterior ensemble members from an ETKF-type method when the size of the forecast ensemble has been synthetically increased from K members to KL members. To better assess the potential value of the GETKF, alternative methods for creating just K analysis members from KL members were also examined. These alternative methods included the well-established perturbed observation method, a stochastic subsampling of the analysis distribution implied by the KL member posterior ensemble, a deterministic subsampling approach, and a demodulation approach.

In tests with a statistical model that used 50 raw ensemble members to assimilate a vertical profile of observations, each of which was an integral of the state and in which the true suboptimal analysis error covariance matrix was perfectly known, it was found that the GETKF produced significantly more accurate analysis error covariance matrices than any of the aforementioned alternatives.

In cycling data assimilation tests with a newly developed 80-variable storm-track version of the Lorenz-96 model and observations that were integrals of the state, the following results were obtained:

(i) Model space localization outperformed observation space localization.
(ii) The GETKF method for obtaining a K-member posterior ensemble from a KL-member prior ensemble resulted in lower mean square analysis errors than either the demodulation or perturbed observation methods.
(iii) If the GETKF's posterior adjustment factor was set equal to unity rather than the value given by (30), GETKF's performance was identical to that obtained when modulated ensembles were used in the serial EnSRF and the serial EnSRF's modified gain was used to obtain K posterior perturbations.
(iv) The GETKF gave superior or equivalent performance to the EnSRF when (30) was used to set the GETKF's posterior adjustment factor a. The superior performance was confined to localization length scales larger than the optimal localization length scale. Intriguingly, at the optimal localization length scale, the average value of a was approximately equal to 1.

In dynamical systems that have a richer range of scales than the simple storm-track model considered here, it can be impractical to optimally tune the localization length scale for all the phenomena likely to occur. In such situations, the lack of sensitivity of GETKF performance to localization length scale could lend it advantages over the EnSRF.

Within the context of LETKFs, our simple model results suggest that the GETKF ensemble update algorithm should replace the ETKF ensemble update when modulation product ensembles have been used for vertical model space localization. Penny et al. (2015) have demonstrated how the removal of vertical localization allows the LETKF to update entire vertical columns of state variables simultaneously. The GETKF with ensembles modulated in the vertical also simultaneously updates entire vertical columns of state variables, but in contrast to Penny et al. (2015), it incorporates vertical *model space* localization. For observations of variables

that are vertical integrals of the state such as satellite-based radiance observations, the vertical "location" of the observation is ill-defined. This makes observation space localization particularly problematic. Our experiments together with those of Campbell et al. (2010) and Whitaker (2016) have found that model space localization was more effective than observation space localization when assimilating observations of variables that are vertical integrals of the state.

Within the context of deterministic EnKFs that assimilate observations serially and employ model space vertical localization through a modulation product ensemble expansion, our results suggest that performance might be improved by replacing the one-at-a-time serial assimilation of a vertical column of observations by an "all at once" assimilation of the entire vertical column of observations using the GETKF. In such systems, the LETKF could achieve ensemble covariance localization in the horizontal using horizontal-distance-dependent observation error variance inflation while a serial deterministic EnKF could achieve it using localization functions that were solely a function of horizontal distance.

In future work, we plan to apply a local volume version of the GETKF, using modulation product ensembles to assimilate satellite radiances with vertical localization in model space. Preliminary experiments using a serial assimilation approach (Whitaker 2016) have shown this approach to significantly enhance the ability of ensemble methods to extract information from satellite radiances. Apart from the potential skill gains mentioned in result iv above, it is possible that the local GETKF version of the algorithm will be found to be computationally more efficient than the serial filter in atmospheric applications because 1) the number of observations typically far exceeds the number of modulated ensemble members and 2) the matrix $\mathbf{A}$ in (6) and its eigenvalue decomposition (7) required to compute both the Kalman and modified Kalman gains need only be done once for each update of an entire vertical column.

Acknowledgments. CHB gratefully acknowledges funding support from the Chief of Naval Research through the NRL Base Program (PE 0601153N). JSW and LL acknowledge the support of the Disaster Relief Appropriations Act of 2013 (P.L. 113-2) that funded NOAA Research Grant NA14OAR4830123.

APPENDIX

Analysis Error Covariance Matrix in the Presence of a Suboptimal Gain

Here, we consider the class of data assimilation schemes for which

$$\overline{\mathbf{x}^a} = \overline{\mathbf{x}^f} + \mathbf{K}[\mathbf{R}^{-1/2}\mathbf{y} - \overline{\tilde{H}(\mathbf{x}^f)}]. \tag{A1}$$

Subtracting the truth from both sides of this equation gives

$$\boldsymbol{\varepsilon}^a = \boldsymbol{\varepsilon}^f + \mathbf{K}[\mathbf{R}^{-1/2}\boldsymbol{\varepsilon}^o - \tilde{H}\boldsymbol{\varepsilon}^f], \tag{A2}$$

where $\boldsymbol{\varepsilon}^a = \overline{\mathbf{x}^a} - \mathbf{x}^t$, $\boldsymbol{\varepsilon}^f = \overline{\mathbf{x}^f} - \mathbf{x}^t$, $\boldsymbol{\varepsilon}^o = \mathbf{y} - \mathbf{y}^t$, and $\tilde{H}\boldsymbol{\varepsilon}^f = [\tilde{H}(\mathbf{x}^f) - \mathbf{R}^{-1/2}\mathbf{y}^t]$. Assuming that there is zero covariance between the observation and forecast errors $[\langle\boldsymbol{\varepsilon}^o(\tilde{H}\boldsymbol{\varepsilon}^f)^{\mathrm{T}}\rangle = \mathbf{0}]$, (A2) then implies

$$\mathbf{P}^a = \langle\boldsymbol{\varepsilon}^a\boldsymbol{\varepsilon}^{a\mathrm{T}}\rangle = \mathbf{P} - \mathbf{K}\tilde{H}\mathbf{P} - (\mathbf{K}\tilde{H}\mathbf{P})^{\mathrm{T}} + \mathbf{K}[\tilde{H}\mathbf{P}\tilde{H}^{\mathrm{T}} + \mathbf{I}]\mathbf{K}^{\mathrm{T}},$$
$$\text{where} \quad \mathbf{P} = \langle\boldsymbol{\varepsilon}^f(\boldsymbol{\varepsilon}^f)^{\mathrm{T}}\rangle, \tilde{H}\mathbf{P} = \langle\tilde{H}\boldsymbol{\varepsilon}^f(\boldsymbol{\varepsilon}^f)^{\mathrm{T}}\rangle, \quad \text{and} \quad \tilde{H}\mathbf{P}\tilde{H}^{\mathrm{T}} = \langle\tilde{H}\boldsymbol{\varepsilon}^f(\tilde{H}\boldsymbol{\varepsilon}^f)^{\mathrm{T}}\rangle. \tag{A3}$$

REFERENCES

Anderson, J. L., 2001: An ensemble adjustment Kalman filter for data assimilation. *Mon. Wea. Rev.*, **129**, 2884–2903, doi:10.1175/1520-0493(2001)129<2884:AEAKFF>2.0.CO;2.

——, and L. Lei, 2013: Empirical localization of observation impact in ensemble Kalman filters. *Mon. Wea. Rev.*, **141**, 4140–4153, doi:10.1175/MWR-D-12-00330.1.

Bishop, C. H., and D. Hodyss, 2009: Ensemble covariances adaptively localized with ECO-RAP. Part 2: A strategy for the atmosphere. *Tellus*, **61A**, 97–111, doi:10.1111/j.1600-0870.2008.00372.x.

——, and ——, 2011: Adaptive ensemble covariance localization in ensemble 4D-VAR state estimation. *Mon. Wea. Rev.*, **139**, 1241–1255, doi:10.1175/2010MWR3403.1.

——, and E. A. Satterfield, 2013: Hidden error variance theory. Part I: Exposition and analytic model. *Mon. Wea. Rev.*, **141**, 1454–1468, doi:10.1175/MWR-D-12-00118.1.

——, B. J. Etherton, and S. J. Majumdar, 2001: Adaptive sampling with the ensemble transform Kalman filter. Part I: Theoretical aspects. *Mon. Wea. Rev.*, **129**, 420–436, doi:10.1175/1520-0493(2001)129<0420:ASWTET>2.0.CO;2.

Bonavita, M., M. Hamrud, and L. Isaksen, 2015: EnKF and hybrid gain ensemble data assimilation. Part II: EnKF and hybrid gain results. *Mon. Wea. Rev.*, **143**, 4865–4882, doi:10.1175/MWR-D-15-0071.1.

Burgers, G., P. J. van Leeuwen, and G. Evensen, 1998: Analysis scheme in the ensemble Kalman filter. *Mon. Wea. Rev.*, **126**, 1719–1724, doi:10.1175/1520-0493(1998)126<1719:ASITEK>2.0.CO;2.

Campbell, W. F., C. H. Bishop, and D. Hodyss, 2010: Covariance localization for satellite radiances in ensemble Kalman filters. *Mon. Wea. Rev.*, **138**, 282–290, doi:10.1175/2009MWR3017.1.

Gaspari, G., and S. E. Cohn, 1999: Construction of correlation functions in two and three dimensions. *Quart. J. Roy. Meteor. Soc.*, **125**, 723–757, doi:10.1002/qj.49712555417.

Hamill, T. M., J. S. Whitaker, and S. Snyder, 2001: Distance-dependent filtering of background error covariance estimates in an ensemble Kalman filter. *Mon. Wea. Rev.*, **129**, 2776–2790, doi:10.1175/1520-0493(2001)129<2776:DDFOBE>2.0.CO;2.

Hamrud, M., M. Bonavita, and L. Isaksen, 2015: EnKF and hybrid gain ensemble data assimilation. Part I: EnKF implementation. *Mon. Wea. Rev.*, **143**, 4847–4864, doi:10.1175/MWR-D-14-00333.1.

Hodyss, D., W. Campbell, and J. Whitaker, 2016: Observation-dependent posterior inflation for the ensemble Kalman filter. *Mon. Wea. Rev.*, **144**, 2667–2684, doi:10.1175/MWR-D-15-0329.1.

Houtekamer, P. L., and H. L. Mitchell, 1998: Data assimilation using an ensemble Kalman filter technique. *Mon. Wea. Rev.*, **126**, 796–811, doi:10.1175/1520-0493(1998)126<0796:DAUAEK>2.0.CO;2.

Hunt, B. R., E. J. Kostelich, and S. Szunyogh, 2007: Efficient data assimilation for spatiotemporal chaos: A local ensemble transform Kalman filter. *Physica D*, **230**, 112–126, doi:10.1016/j.physd.2006.11.008.

Kretschmer, M., B. R. Hunt, and E. Ott, 2015: Data assimilation using a climatologically augmented local ensemble transform Kalman filter. *Tellus*, **67A**, 26617, https://dx.doi.org/10.3402/tellusa.v67.26617.

Leng, H., J. Song, F. Lu, and X. Cao, 2013: A new data assimilation scheme: The space-expanded ensemble localization Kalman filter. *Adv. Meteor.*, **2013**, 410812, doi:10.1155/2013/410812.

Lorenz, E. N., and K. A. Emanuel, 1998: Optimal sites for supplementary weather observations: Simulations with a small model. *J. Atmos. Sci.*, **55**, 399–414, doi:10.1175/1520-0469(1998)055<0399:OSFSWO>2.0.CO;2.

Penny, S. G., 2014: The hybrid local ensemble transform Kalman filter. *Mon. Wea. Rev.*, **142**, 2139–2149, doi:10.1175/MWR-D-13-00131.1.

——, D. W. Behringer, J. A. Carton, and E. Kalnay, 2015: A hybrid Global Ocean Data Assimilation System at NCEP. *Mon. Wea. Rev.*, **143**, 4660–4677, doi:10.1175/MWR-D-14-00376.1.

Sommer, M., and T. Janjic, 2017: A flexible additive inflation scheme for treating model error in ensemble Kalman filters. *Proc. 19th European Geophysical Union General Assembly*, Vienna, Austria, EGU2017-7393, http://meetingorganizer.copernicus.org/EGU2017/EGU2017-7393.pdf.

Wang, X., C. H. Bishop, and S. J. Julier, 2004: Which is better, an ensemble of positive–negative pairs or a centered spherical simplex ensemble? *Mon. Wea. Rev.*, **132**, 1590–1605, doi:10.1175/1520-0493(2004)132<1590:WIBAEO>2.0.CO;2.

——, T. M. Hamill, J. S. Whitaker, and C. H. Bishop, 2007: A comparison of hybrid ensemble transform Kalman filter–Optimum interpolation and ensemble square root filter analysis schemes. *Mon. Wea. Rev.*, **135**, 1055–1076, doi:10.1175/MWR3307.1.

Whitaker, J. S., 2016: Performing model space localization for satellite radiances in an ensemble Kalman filter. *20th Conf. on Integrated Observing and Assimilation Systems for the Atmosphere, Oceans, and Land Surface (IOAS-AOLS)*, New Orleans, LA, Amer. Meteor. Soc., P253, https://ams.confex.com/ams/96Annual/webprogram/Paper281727.html.

——, and T. M. Hamill, 2002: Ensemble data assimilation without perturbed observations. *Mon. Wea. Rev.*, **130**, 1913–1924, doi:10.1175/1520-0493(2002)130<1913:EDAWPO>2.0.CO;2.